JGR Solid Earth

RESEARCH ARTICLE
10.1029/2020JB021256

Coupled Rapid Erosion and Foreland Sedimentation Control Orogenic Wedge Kinematics in the Himalayan Thrust Belt of Central Nepal

P. G. DeCelles[1] and B. Carrapa[1]

[1]Department of Geosciences, University of Arizona, Tucson, AZ, USA

Key Points:

- A Miocene-Pliocene erosional bight was rapidly excavated in central Nepal, stalling forward propagation of the Main Boundary thrust
- Sediment from the bight subsequently deposited in the foreland raised initial taper to criticality promoting long-distance thrust propagation
- Coincident erosional hotspots, salient-reentrant couples, and thick foreland sediments suggest future frontal seismic activity

Supporting Information:

Supporting Information may be found in the online version of this article.

Correspondence to:

P. G. DeCelles,
decelles@arizona.edu

Citation:

DeCelles, P. G., & Carrapa, B. (2021). Coupled rapid erosion and foreland sedimentation control orogenic wedge kinematics in the Himalayan thrust belt of central Nepal. *Journal of Geophysical Research: Solid Earth*, *126*, e2020JB021256. https://doi.org/10.1029/2020JB021256

Received 28 OCT 2020
Accepted 2 MAR 2021

Abstract Spatial and temporal coincidence among rapid Pliocene-Holocene bedrock exhumation, development of a topographic bight, abundant monsoonal precipitation, accumulation of anomalously thick proximal foreland basin deposits, and development of an opposite-polarity salient-reentrant couple on the two most frontal major thrust faults in the Himalayan orogenic wedge of central Nepal provide a basis for a model that links these diverse phenomena and could be operating in other parts of the frontal Himalaya. Rapid bedrock erosion is documented by a concentration of young (<5 Ma) low-temperature thermochronologic ages in the Narayani River catchment basin. Where the river exits the Lesser Himalayan Zone, the Main Boundary thrust has a 15-km-amplitude reentrant. Directly south of the reentrant lies the ~50 km wide Chitwan wedge-top basin, which is confined by a large salient on the Main Frontal thrust. Rapid erosion and sediment flux out of the Narayani catchment basin, possibly due to anomalously intense monsoonal precipitation in this topographically depressed region of central Nepal, causes greater flexural subsidence and surface aggradation in the foreland, both of which increase initial wedge taper and render this region more susceptible to anomalous forward propagation of the thrust front. Analysis of the modern and post-early Miocene taper history of the thrust belt suggests that rapid erosion hindered forward propagation of the contemporaneous Main Boundary thrust, but simultaneously produced conditions in the foreland that eventually elevated initial taper to a critical/supercritical value promoting forelandward propagation of the Main Frontal thrust. This analysis has implications for large damaging earthquakes in the Himalaya.

Plain Language Summary The geological history of faulting in the Himalaya is controlled by the distribution of mass in the mountain range and the tectonic forces acting in the ongoing collision between India and Asia. Accordingly, erosion by large rivers, which redistributes mass from the mountain range into the Ganges River basin south of the mountains, may control the locations, shapes, and seismic histories of major Himalayan faults. We show a strong correlation among rapid erosion in central Nepal, extreme precipitation, anomalous sediment deposition in the basin to the south, and peculiarities in the shapes and movement histories of the two largest faults along the southern flank of the range. Our findings have implications for the history of large earthquakes along the front of the Himalaya. In particular, spatial correlations among large erosional basins in the Himalaya, thick sediment accumulations to the south, and abrupt deflections in the shapes of major faults point to enhanced seismic potential along the mountain front.

1. Introduction

The importance of large-scale thrust faults in the development of orogenic belts has been recognized since the mid-1800s (Bertrand, 1884; Peach et al., 1888, 1907; Schardt, 1898; cf., Şengör & Bernoulli, 2011 for a review of early Alpine literature). Physical mechanisms by which large coherent thrust sheets are emplaced upon the rocks beneath them posed a dilemma (Smoluchowski, 1909; see also; Engelder, 1990; Price, 1988) until the overall wedge-shaped cross-section of most thrust belts became more clear (Bally et al., 1966; Price, 1973, 1988) and the effects of elevated fluid pressures (Hubbert & Rubey, 1959) and the gravitational body force acting on elevated rocks in the orogenic wedge were realized (Chapple, 1978; Dahlen, 1984, 1990; D. Davis et al., 1983; D. Elliott, 1976). Together with a driving plate tectonic force, gravity acting on elevated orogenic rocks drives the orogenic wedge forward against resisting basal shear forces (e.g., Molnar & Lyon-Caen, 1988; Willett, 1992). Analytical, numerical, and analog models that simulate or embody this

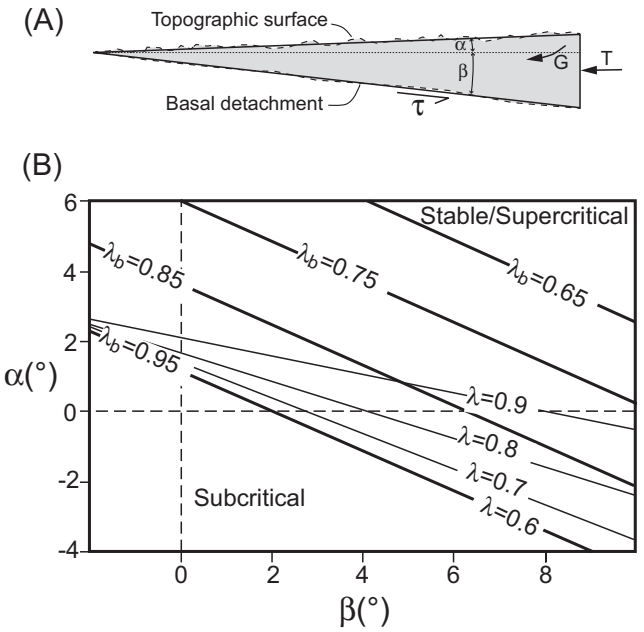

Figure 1. (a) Schematic diagram illustrating a cross-sectional view of the basal detachment angle (β) and upper surface slope (α) of a typical fold-thrust belt at large scale; driving (gravity, G; and tectonic, T) and resisting forces (friction, τ) are annotated. (b) Lines of critical taper in terms of basal slope (β) and upper surface slope (α), calculated for different values of pore-fluid pressure ratios within the orogenic wedge (λ) and along the base of the wedge (λ_b). Values of internal wedge pore-fluid pressure ratio are shown for only $\lambda_b = 0.95$, but each bold line would have a similar set of curves depending on λ. Each line separates the region of subcritical wedge taper from supercritical wedge taper. After Willett and Schlunegger (2010).

concept are called critical taper models because they parameterize orogenic wedges in terms of the taper angle of the orogenic wedge, which is the sum of the surface angle (α) and basal detachment angle (β) (Figure 1a; e.g., Chapple, 1978; Dahlen, 1984; D. Davis et al., 1983); when the taper angle is sufficiently high, stresses within and on the wedge are balanced and the wedge is considered to be in a critical (at failure) state. Functionally critical, supercritical, and subcritical tapers result from combinations of numerous variables and control the kinematics of brittle and perfectly plastic orogenic wedges (Figure 1b; Chapple, 1978; D. Davis et al., 1983; DeCelles & Mitra, 1995; Hilley & Strecker, 2004; Mitra, 1997; Mulugeta, 1988; Platt, 1986; Stockmal, 1983; Stockmal et al., 2007; Willett, 1992, 1999; Williams et al., 1994).

While helping to explain many aspects of both modern (Carena et al., 2002; Chalaron et al., 1995; Mukul, 2010; Suppe, 2007) and ancient (Braathen et al., 1999; DeCelles & Mitra, 1995; Horton, 1999; Meigs & Burbank, 1997; Mitra, 1997) orogenic wedge behavior, critical taper models themselves would seem to introduce yet another dilemma, insofar as an orogenic wedge is moveable only if it has sufficient taper and yet large parts of active orogenic wedges have very low tapers. This problem is acute at the front of the thrust belt, where it propagates into rocks and sediments in the undeformed foreland basin that have a surface angle that is either very low or even negative (sloping back toward the thrust belt hinterland). This low- or negative-α (Fuller et al., 2006) situation prevails at the fronts of all thrust belts and accretionary prisms and poses a fundamental problem for how thrust belts are able to propagate forward (Boyer, 1995; Fuller et al., 2006; Muñoz et al., 1994; Pieri, 1989; Simpson, 2010; Stockmal et al., 2007; Willett & Schlunegger, 2010). Some of these cases can be explained by the presence of extremely weak rocks, such as salt, involved in the basal detachment (e.g., Dahlen, 1990; D. M. Davis & Engelder, 1985; Ford, 2004; Jaumé & Lillie, 1988; Willett & Schlunegger, 2010), but many foreland basin fills lack such lithologies. In this paper, we combine concepts of critical taper models operating at low taper values with low-temperature thermochronological and geological data to analyze the central Nepal segment of the Himalayan fold-thrust belt in terms of its late Miocene-present kinematic behavior. We find that functionally critical taper at the front of the Himalayan orogenic wedge is controlled mainly by flexural subsidence and sediment aggradation, both of which increase initial taper (Boyer, 1995; Ford, 2004), defined as the sum of α_0 and β_0, in the most proximal part of the Gangetic foreland basin. The trade-off between wedge erosion and sediment aggradation in front of the wedge partly controls the rate at which the thrust belt propagates forward. This has potential significance for kinematics of thrust belt propagation in general and for seismic hazards.

2. Tectonic and Geologic Setting

2.1. Structure and Stratigraphy of the Himalayan Orogenic Wedge

The Himalayan thrust belt in Nepal and southern Tibet is a southward tapering orogenic wedge composed of Paleoproterozoic to Neogene rocks carried southward relative to northward underthrusting India by thrust faults that branch upward from the Himalayan basal décollement, which slopes upward from a depth of ~55 km beneath the northern Himalaya to the topographic surface along or near the Main Frontal thrust (Figures 2 and 3; Duputel et al., 2016; Gao et al., 2016; Hauck et al., 1998; Nábělek et al., 2009; Schulte-Pelkum et al., 2005). From north to south, the thrust belt is divided into four topographic zones referred to as the Tibetan Himalayan, Greater Himalayan, Lesser Himalayan, and Sub-Himalayan Zones (Hodges, 2000). In central Nepal boundaries of these zones more or less follow major faults/shear zones, including the South Tibetan fault system, Main Central thrust, Main Boundary thrust, and the Main Frontal thrust (Hodges, 2000; S. B. Shrestha et al., 1987a; Stöcklin, 1980; Figure 2). Another major fault, the Ramgarh thrust, is

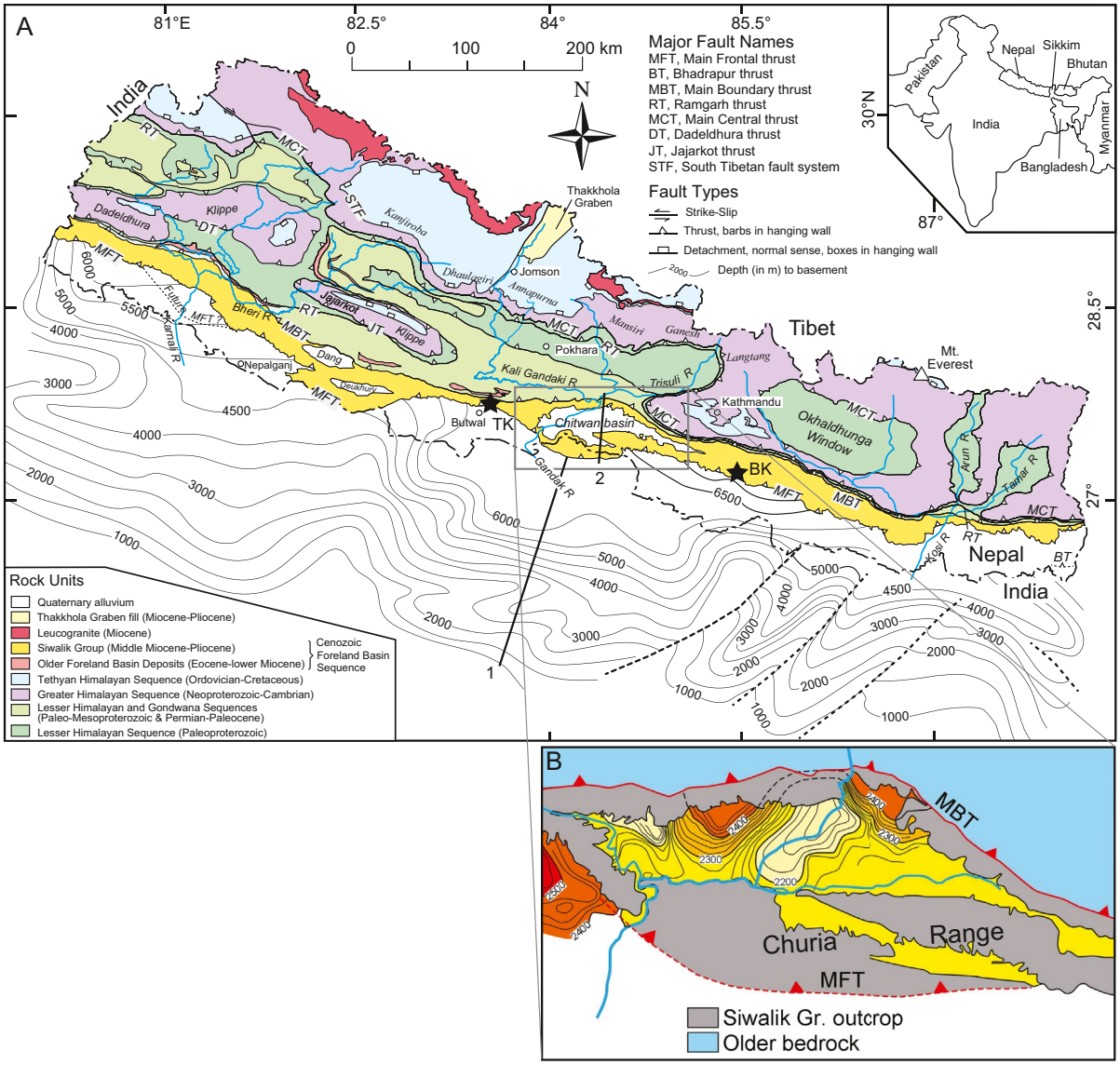

Figure 2. (a) Generalized geological map of Nepal (after DeCelles et al., 2020) showing tectonostratigraphic units and major faults, and highlighting location of Chitwan wedge-top basin. Also shown are contours of depth to basement beneath the foreland basin (after Duvall et al., 2018; Raiverman et al., 1983). Geology is depicted only for Nepal, and only the depth of basement is depicted for northern India. Line 1 is transect used to create a basin fill profile for comparison with calculated flexural profiles in Figure 14. Line 2 is location of cross-section in Figure 3. Stars indicate locations of Tinau Khola (TK) and Bakiya Khola (BK) sections of the Siwalik Group (see text). (b) Isopach contours of Siwalik Group (in shades of yellow and orange) in Chitwan wedge-top basin (Friedenreich et al., 1994).

located in the Lesser Himalayan Zone a few kilometers structurally beneath the Main Central thrust (DeCelles et al., 2020; Pearson & DeCelles, 2005; Robinson & Martin, 2014; Robinson et al., 2006; Srivastava & Mitra, 1994).

Five packages of rocks compose the Himalayan thrust belt in Nepal (DeCelles et al., 2020; Hodges, 2000; Martin, 2017): from oldest to youngest these are the Lesser Himalayan Sequence (LHS); Greater Himalayan Sequence (GHS); Tethyan (or Tibetan) Himalayan Sequence (THS); Gondwana Sequence (GS); and the Cenozoic Foreland Basin Sequence (CFBS). The northern half of the thrust belt (Tibetan Himalayan Zone) is dominated by the THS, with local outcrops of GHS exposed in the North Himalayan domes. The THS is composed of mostly unmetamorphosed Ordovician-Cretaceous carbonate and fine-grained siliciclastic strata. The GHS sits between the Main Central thrust and the South Tibetan detachment and is composed of Neoproterozoic-early Ordovician amphibolite facies metasedimentary and metaigneous rocks and Neogene

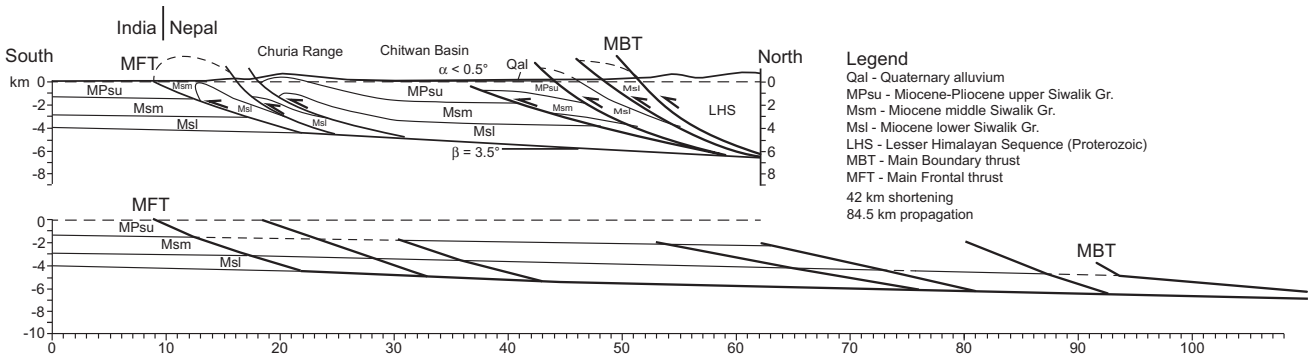

Figure 3. Deformed-state (above) and restored-state cross-sections for the Main Frontal thrust system in the Chitwan wedge-top basin area. Line of cross-section shown in Figure 2. Based on unpublished seismic data from Nepal Department of Mines and Geology and Petro-Canada (cf., Friedenreich et al., 1994; Slind, 1993).

leucogranites. The LHS crops out in the Lesser Himalayan Zone and is composed of Paleo- to Mesoproterozoic greenschist to lower amphibolite facies metasedimentary and metaigneous rocks. The GS crops out in the Lesser Himalayan Zone and consists of Permian-Paleocene sandstone, shale, and glacial diamictite. The CFBS crops out in the Tibetan Himalayan (along and near the Yarlung suture), Lesser Himalayan, and Sub-Himalayan Zones. In the Tibetan Himalayan Zone the CFBS consists of Paleocene-Eocene deep marine to deltaic sandstone and shale (DeCelles et al., 2014; Ding et al., 2005; Hu et al., 2015; Zhu et al., 2005); in the Lesser Himalayan Zone it comprises Eocene and lower Miocene limestone, shale, sandstone, and minor conglomerate of the Bhainskati and Dumri Formations (DeCelles et al., 2004); and in the Sub-Himalayan Zone it consists of Middle Miocene-Pliocene siltstone, sandstone and conglomerate of the Siwalik Group (Ojha et al., 2009). The Siwalik Group in Nepal is divided into informal lower, middle and upper members (DeCelles et al., 1998; Quade et al., 1995).

The traces of the Main Boundary and Main Frontal thrusts are relatively straight and continuous, running parallel to the regional trend of Himalayan topography (Figure 2). Plan-view shapes of the Main Central and Ramgarh thrusts are more irregular, with large southward and northward projecting salients and reentrants, as well as erosional-remnant klippen and structural windows. The irregular shape of the Main Central and Ramgarh thrust traces owes to the growth of structural culminations in the Lesser Himalayan duplex, a large antiformal structure that runs nearly the entire length of the Himalayan thrust belt in India, Nepal, and Bhutan (e.g., DeCelles et al., 1998, 2016, 2020; Long et al., 2011; Mitra et al., 2010; Robinson & Martin, 2014; Robinson et al., 2006; Srivastava & Mitra, 1994; Webb et al., 2011; Yin et al., 2010). GHS rocks cover most of the southern half of the thrust belt in eastern Nepal, but in central and western Nepal the GHS has been widely eroded off the crest of the Lesser Himalayan duplex (Figure 2). The Jajarkot and Dadeldhura klippen are erosional remnants of GHS rocks in western Nepal, and between the eastern terminus of the Jajarkot klippe and the western edge of the Kathmandu salient lies a region in which GHS rocks have been almost completely eroded northward to the foot of the Annapurna Range (Figure 2).

The southern part of the Himalayan thrust belt is a typical example of an active thrust belt propagating into its undeformed low- to negative-α (Fuller et al., 2006; Willett & Schlunegger, 2010) foreland basin. This part of the orogenic wedge is composed of several (variable along strike) thrust sheets of the Siwalik Group carried by faults in the Main Frontal thrust system (Chalaron et al., 1995; Mugnier et al., 1994, 1999, 2004). Surface dip data, stratigraphic sections, and sparse reflection seismic data demonstrate that the faults carrying these thrust sheets branch upward from the Himalayan basal décollement (Almeida et al., 2018; DeCelles et al., 1998; Mugnier et al., 1994, 1999, 2004, 2005; Powers et al., 1998; Schelling & Arita, 1991), the surface manifestation of which is the Main Frontal thrust (Figure 3). The oldest stratigraphic unit in the hanging wall of the Main Frontal thrust is the lower member of the Siwalik Group; this implies that the frontal part of the thrust belt is detached at the top of the lower Miocene Dumri Formation in the subsurface. South of the Main Frontal thrust lies the actively subsiding Himalayan foreland basin, beneath which Indian basement has been flexed downward ~5–6.5 km below sea level directly adjacent to the Main Frontal thrust (Figure 2; Burbank et al., 1996; Duvall et al., 2018; Lyon-Caen & Molnar, 1985; Raiverman et al., 1983).

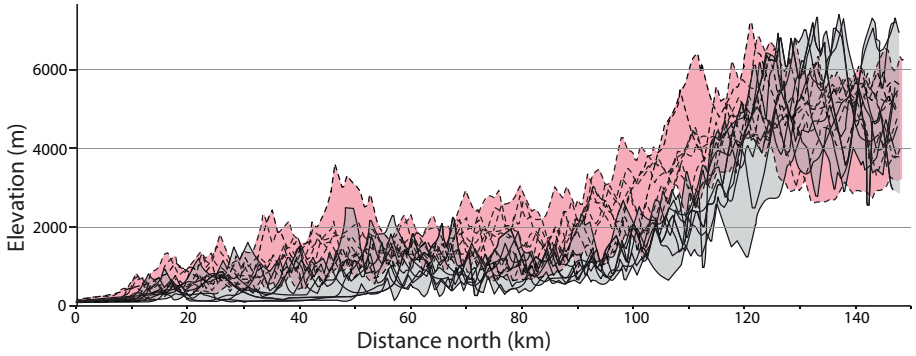

Figure 4. Topographic profiles (see Figure S1 for locations) in central Nepal. Solid line profiles with gray fill are within the erosional bight and dashed profiles with pink fill are outside of the erosional bight.

Geomorphic and reflection seismic evidence exists for local, active blind thrusting in the subsurface south of the Main Frontal thrust (e.g., Bhadrapur thrust in Figure 2; Almeida et al., 2018; Delcaillau, 1997; Duvall et al., 2020).

2.2. Geomorphology

Topographic profiles oriented parallel to the shortening direction (~N18°E) in the Himalaya exhibit two general forms: upward convex and upward concave (e.g., Bookhagen & Burbank, 2010; Duncan et al., 2003). Upward convex profiles characterize regions in which GHS rocks are widely preserved (Bhutan, eastern Nepal; Adams et al., 2016; Burbank et al., 2012; Duncan et al., 2003; Grujic et al., 2006). The region of central Nepal between the western side of the Kathmandu salient and the eastern side of the Dadeldhura klippe contains almost no GHS rocks south of the Annapurna Range, and topographic profiles in the shortening direction are concave upward (Figure 4). We will refer to this relatively deeply eroded region in central Nepal as the "erosional bight" (Figure 5). The erosional bight occupies approximately the southern third of the ~32,000 km^2 Narayani River catchment (Andermann et al., 2012), which gathers the waters of the Kali Gandaki, Modi, Madi, Burhi Gandaki, Marsyangdi, and Trisuli Rivers along with hundreds of smaller rivers and streams that collectively drain the precipitous south flanks of the Dhaulagiri, Annapurna, Mansiri, Ganesh, and Langtang Himal ranges (Figures 2 and 5). The northern edge of the erosional bight coincides

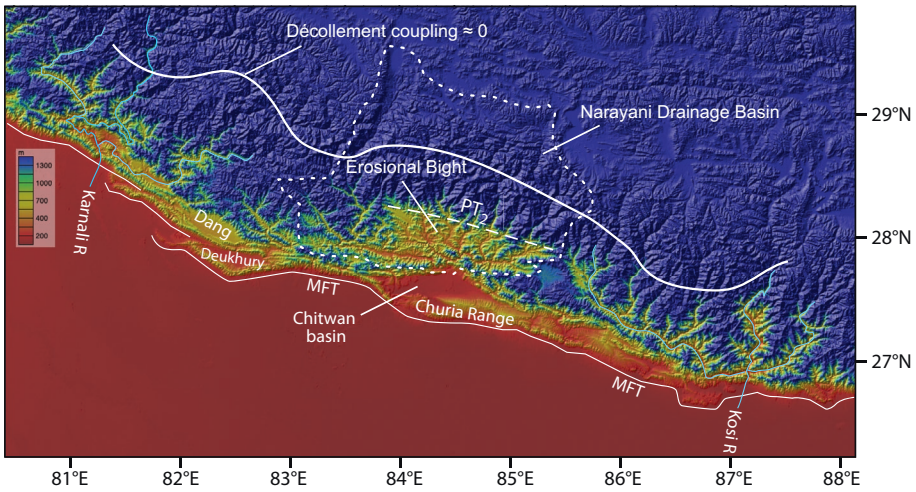

Figure 5. Digital elevation model (GeoMapApp, GMRT) of Himalayan thrust belt in central Nepal, highlighting the erosional bight, the Main Frontal thrust (MFT), Narayani drainage basin, physiographic transition PT_2 of Wobus et al. (2003), the approximate line north of which the geodetically derived interseismic coupling along the basal décollement drops to near zero (Ader et al., 2012), the Dang, Deukhury, and Chitwan wedge-top basins, and major rivers of the Karnali and Kosi River watersheds.

with a nearly straight, ~235 km long band of steep fluvial channel segments (e.g., Cannon et al., 2018; Johnston et al., 2020; Wobus et al., 2003) and abrupt hillslope steepening referred to as physiographic transition "PT_2" by Hodges et al. (2001) and Wobus et al. (2003). The Narayani basin protrudes into topographic Tibet at its northwestern and northeastern corners by virtue of the high elevation Thakkhola and Gyirong grabens, respectively, which are Miocene-Holocene extensional basins bounded by steep normal faults that strike roughly north-south and dip inward toward the Narayani basin (Colchen, 1999; DeCelles et al., 2018; Hurtado et al., 2001; Shen et al., 2016; Xu et al., 2012). The northern part of the Narayani basin between the two grabens encompasses the >8 km high Annapurna Range as well as the region of high peaks and >5 km base-elevations in northern central Nepal and southern Tibet. At its downstream end, the Narayani crosses the Main Frontal thrust and enters the open foreland basin as the Gandak River, which is a major tributary of the Ganges River. Discharge in the Gandak River at the mountain front is 5.2×10^{10} m^3/yr (Alford, 1992; Rao, 1973), and sediment load is 8.2×10^7 t/yr (Sinha & Friend, 1994).

In central Nepal, the trace of the Main Boundary thrust exhibits a prominent northward reentrant, with an amplitude of ~15 km measured in a northeastward direction (Figure 2b). The Narayani River crosses the Main Boundary thrust at the apex of this reentrant and enters the Chitwan wedge-top basin. Along its southern flank the Chitwan basin is confined by the Churia Range, which consists of uplifted Siwalik Group in the hanging wall of the Main Frontal thrust (Figures 2 and 3). The Chitwan wedge-top basin is ~94 km long east to west, and ~51 km across from northeast to southwest. The basin is partitioned by a sub-range composed of Siwalik Group strata uplifted above splay thrusts north of the Main Frontal thrust. The mean slope of the Narayani River along its ~55 km valley length in the Chitwan basin is ~0.06°. Along a direct northeast-southwest line from the Narayani exit to the north flank of the Churia Range, the basin surface slopes ~0.32°. The northeast-to-southwest mean slope of the proximal foredeep depozone from the apex of the Chitwan salient to the Ganges River is 0.017°; from the apex of the salient to the Gandak River (about 16 km), the mean slope is ~0.1°.

The trace of the Main Frontal thrust is a near mirror image of the Main Boundary thrust, forming a prominent southward projecting salient. Structural considerations indicate that the Main Boundary thrust reentrant is not merely the result of erosion by the Narayani River because its amplitude is too great (~15 km); given the ~45°NE dip of the Main Boundary thrust and topography on either side of the Narayani exit canyon, erosion alone would produce an upstream "V" with a map-view amplitude of no more than ~3 km. Hence, the shape of the trace of the Main Boundary thrust must reflect less forward propagation of the thrust in the vicinity of Chitwan basin. In contrast, but for similar reasons, the salient in the Main Frontal thrust trace directly south of Chitwan basin must reflect greater forward propagation of the thrust front in this region. Other areas in Nepal where the trace of the Main Frontal thrust bulges southward include along the south side of the Dang and Deukhury valleys in western Nepal (Figures 2 and 5; Mugnier et al., 1999) and the area just southwest of the exit gorge of the Kosi/Arun River in eastern Nepal. Additionally, the newly discovered Bhadrapur thrust in southeasternmost Nepal (Figure 2) may represent an actively propagating new imbricate of the Main Frontal thrust system (Duvall et al., 2020).

The northern part of the Gangetic foreland basin is occupied by fluvial megafans, alluvial fans, and numerous small fluvial systems that are actively depositing boulder- to silt-sized clastic sediment (e.g., Chakraborty et al., 2010; DeCelles & Cavazza, 1999; H. Singh et al., 1993; Sinha & Friend, 1994; Sinha et al., 1996; Wells & Dorr, 1987). Elevations of the southward and eastward sloping active landscape surface range from maxima of ~150–225 m adjacent to the frontal orogenic topography, down to ~30–105 m along the axial eastward flowing Ganges River.

2.3. Precipitation

Precipitation in the Nepalese Himalaya is dominated by the Indian summer monsoon, with 54%–88% of annual rainfall (highly dependent on location) coming between June and September (Figure 6a; Andermann et al., 2012; Bohlinger & Sorterberg, 2017; M. Shrestha, 2000). The south faces of the high ranges in central Nepal are the wettest (Bohlinger & Sorterberg, 2017; Bookhagen & Burbank, 2010; Ichiyanagi et al., 2007; Islam et al., 2010), with mean monsoon rainfall of ~3,000–4,500 mm (Bohlinger & Sorterberg, 2017). Bookhagen and Burbank (2010) calibrated Tropical Rainfall Measurement Mission (TRMM) data with data from ground stations and reported annual means over the period 1998–2007, revealing strong

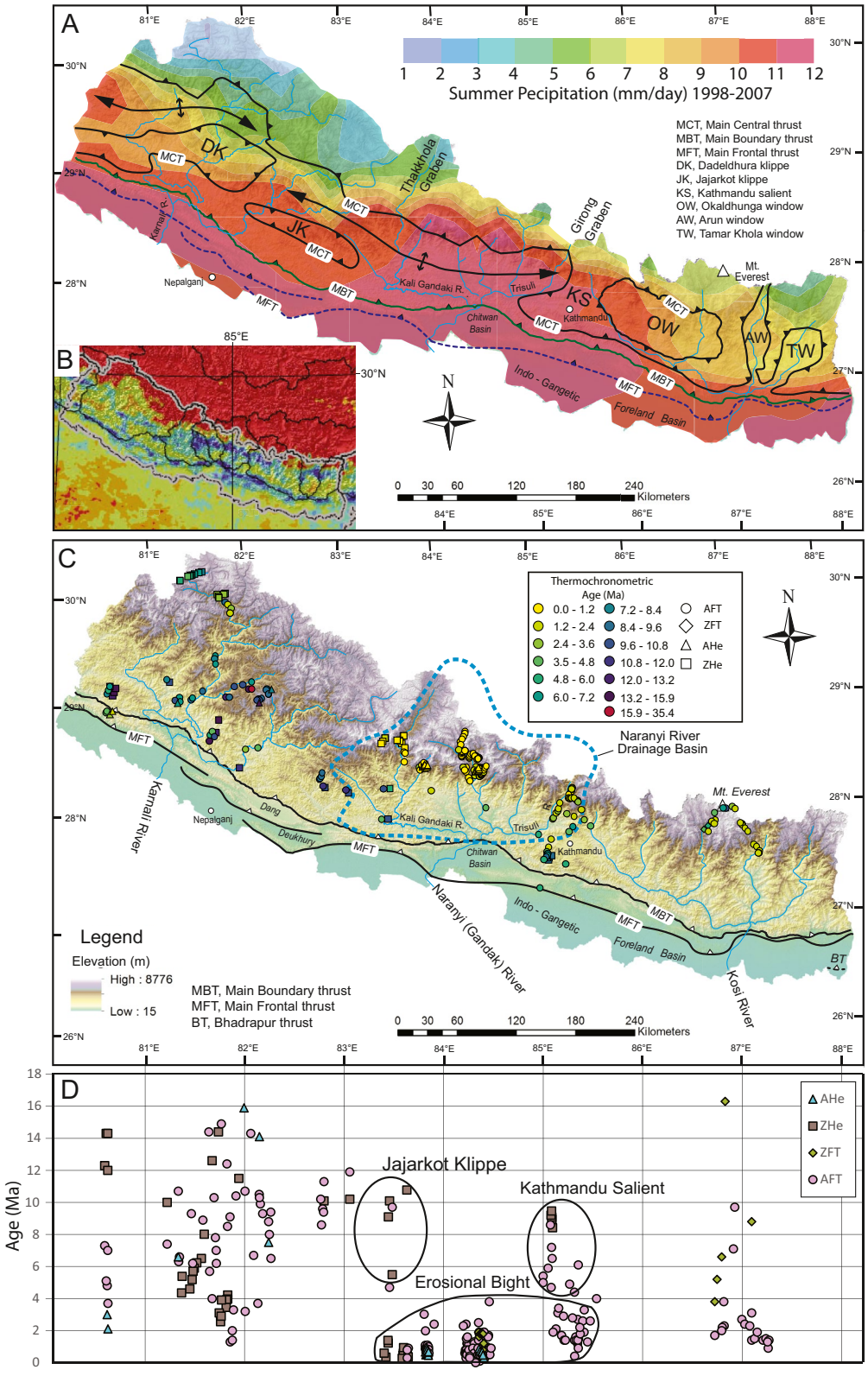
A
Summer Pecipitation (mm/day) 1998-2007
1 2 3 4 5 6 7 8 9 10 11 12
MCT, Main Central thrust
MBT, Main Boundary thrust
MFT, Main Frontal thrust
DK, Dadeldhura klippe
JK, Jajarkot klippe
KS, Kathmandu salient
OW, Okaldhunga window
AW, Arun window
TW, Tamar Khola window
Thakkhola Graben
Girong Graben
Karnali R.
Nepalganj
Kali Gandaki R.
Trisuli
Kathmandu
Chitwan Basin
Mt. Everest
Indo - Gangetic
Foreland Basin
B
C
Thermochronometric Age (Ma)
0.0 - 1.2
1.2 - 2.4
2.4 - 3.6
3.5 - 4.8
4.8 - 6.0
6.0 - 7.2
7.2 - 8.4
8.4 - 9.6
9.6 - 10.8
10.8 - 12.0
12.0 - 13.2
13.2 - 15.9
15.9 - 35.4
AFT
ZFT
AHe
ZHe
Naranyi River Drainage Basin
Karnali River
Dang
Deukhuri
Naranyi (Gandak) River
Kosi River
BT
Legend
Elevation (m)
High : 8776
Low : 15
MBT, Main Boundary thrust
MFT, Main Frontal thrust
BT, Bhadrapur thrust
0 30 60 120 180 240 Kilometers
D
Age (Ma)
Jajarkot Klippe
Kathmandu Salient
Erosional Bight
AHe
ZHe
ZFT
AFT

south-to-north gradients in rainfall from the wet Gangetic plains to the dry Tibetan Plateau (Figure 6b). An east-to-west decreasing gradient in precipitation all along the Himalaya has been suggested by Hirschmiller et al. (2014). In detail, mean annual rainfall (1998–2007) in Nepal is concentrated in two bands (Figure 6b): one approximately along the topographic front; and a second band, restricted to the erosional bight in central Nepal, along the topographic transition between the Lesser and Greater Himalayan Zones (Bookhagen & Burbank, 2010; Burbank et al., 2012). Average July peak-monsoon precipitation (Islam et al., 2010) over the period 1998–2007 shows a strong high in central Nepal overlapping the erosional bight and the southern half of the Narayani drainage basin (Figure 6a). Western, and to some extent eastern, Nepal are comparatively dry, consistent with greater preservation of Greater Himalayan rocks in the hanging wall of the Main Central thrust.

2.4. Himalayan Orogenic Wedge Taper in Central Nepal: Present and Past

2.4.1. Present Taper

Taper of the Himalayan orogenic wedge in Nepal is sparsely documented. Regional surface slope is readily measured from topographic maps and digital elevation models. To determine α values, we constructed 16 topographic profiles (Figure 7) using digital elevation data from GeoMapApp (Global Multi-Resolution Topography) spaced ~16.5 km apart and trending N18.5°E, which is approximately parallel to the shortening direction determined by geodetic studies (Bilham et al., 1997; Jouanne et al., 2004; Larson et al., 1999; Wang & Zhang, 2001). Seven of these profiles cross the Chitwan wedge-top basin and the remainder are northwest and southeast along strike from the Chitwan area (Figure S1). Each profile is ~150 km long and consists of 500–700 elevation values. Bezier curves (splines) were fit to the data and then divided into 3–4 approximately linear segments whose deviations from horizontal were measured (Figure 7). The orogenic wedge is divisible into sectors depending on α values: (1) in profiles that cross the Chitwan basin (profiles 7–13, Figure 7), α values of ~0.4°–0.55° are characteristic south of the Greater Himalayan part of the wedge, and α values of 5.3°–15.8° (average of ~7.6°) are typical in the Greater Himalaya north of PT_2; (2) in the nine profiles (1–6 and 14–16) outside of the Chitwan region (Figure 7), the Lesser Himalayan and Greater Himalayan sectors have average α values of ~1.6° and ~7.4°, respectively. In several profiles, short segments of negative α values are present north of the Lesser Himalayan Mahabharat Range.

The location of the basal décollement of the Himalayan orogenic wedge is constrained in only a few places: (1) by earthquake locations in the region of the 2015 Gorkha events (J. R. Elliott et al., 2016); (2) by broad-band seismic modeling of P- to S-receiver functions (Duputel et al., 2016; Nábělek et al., 2009; Schulte-Pelkum et al., 2005); (3) by reflection seismic profiles beneath the Tibetan Himalayan Zone (Gao et al., 2016; Hauck et al., 1998) and beneath the modern foreland basin and frontmost part of the orogenic wedge (Almeida et al., 2018; Caldwell et al., 2013; Duvall et al., 2020); and (4) by a number of structural cross-sections that are based on surface measurements of dip and dip direction along with thicknesses of stratigraphic units that make up the thrust belt (e.g., DeCelles et al., 2020; Khanal & Robinson, 2013; Robinson & Martin, 2014). In central Nepal, we estimated β values on the basis of seven different sources of information: Three interpretations of passive-source broadband seismic profiles (Duputel et al., 2016; Nábělek et al., 2009; Schulte-Pelkum et al., 2005); three balanced cross-sections based on surface data but partly constrained at depth by reflection seismic data (Friedenreich et al., 1994) and the same seismic profiles and earthquake focal mechanisms mentioned above (e.g., DeCelles et al., 2020; Khanal & Robinson, 2013); and

Figure 6. (a) Simplified tectonic map of Nepal showing major thrust faults (barbed lines) and approximate trends of structural culminations on the Lesser Himalayan duplex (antiform symbols) overlain by July (peak monsoon) precipitation from calibrated TRMM 3B42 data averaged over the years 1998–2007 (after Islam et al., 2010). Note the northward incursion of high precipitation in central Nepal erosional bight. Inset lower left (b) shows mean annual rainfall from calibrated TRMM 2B31 data averaged from 1998 to 2007 from Bookhagen and Burbank (2010). Color scale is approximately opposite to that of Islam et al. (part a), with dark blue being highest rainfall amount. (c) Digital elevation model of Nepal (by T.P. Ojha), showing apatite fission track and apatite and zircon (U-Th)/He thermochronological ages, locations of the Main Boundary (MBT) and Main Frontal thrusts (MFT), the Bhadrapur thrust (BT, Duvall et al., 2020), Chitwan, Dang, and Deukhury wedge-top basins, and major rivers of three main watersheds of Nepal (Karnali, Gandak, and Kosi). Published data used in this compilation are provided in Table S1. (d) Plot of ages versus longitude keyed to longitudes in part (c) showing overlap of youngest ages (of all types) in the erosional bight and deep valleys of the Annapurna Range that drain into the bight. Ages from outside the bight that overlap longitudinally are shown by ellipses labeled Jajarkot klippe and Kathmandu salient.

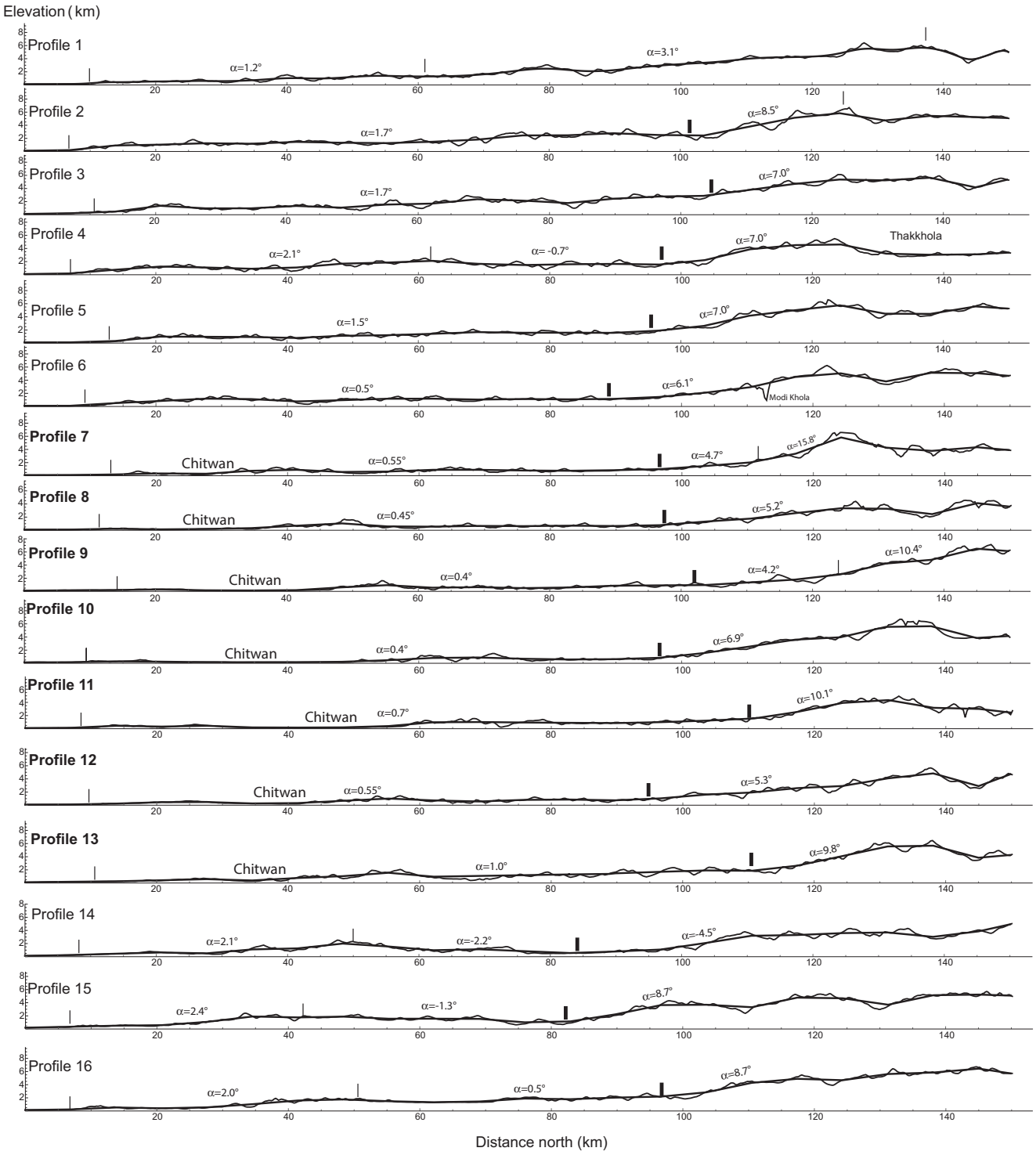

Figure 7. Topographic profiles (irregular lines) fitted with splines (smoother lines) and annotated with average values of surface slope (α). Profiles 7–13 are from within the erosional bight and annotated with location of Chitwan wedge-top basin; all other profiles are outside of the bight. Profile locations in Figure S1. Vertical tick marks bound segments with different α values as discussed in the text. Bold ticks denote approximate southern edge of Greater Himalayan Zone, characterized by an abrupt increase in α.

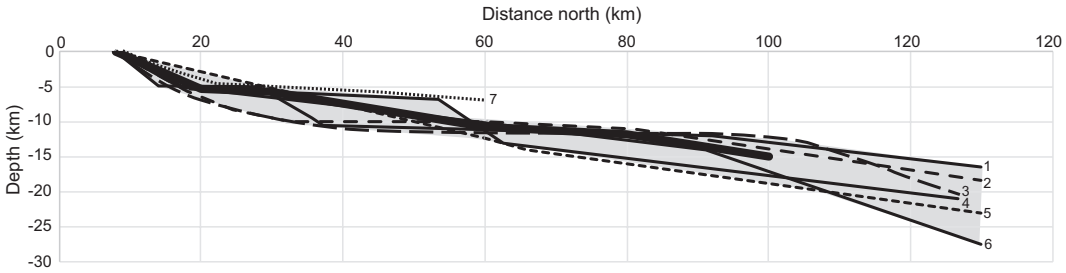

Figure 8. Cross-section profile across the central Nepal thrust belt showing interpreted locations of the basal Himalayan décollement in publications listed. Numbered profiles correspond to the following sources: 1, DeCelles et al. (2020); 2, Nábělek et al. (2009); 3, Duputel et al. (2016); 4, Khanal and Robinson (2013); 5, Schulte-Pelkum et al. (2005); 6, Elliott et al. (2016); 7, Figure 3 of this paper. Gray area indicates complete range of interpretations and bold line is our mean approximation. See text for discussion.

the study of J. R. Elliott et al. (2016), which combined earthquake locations and geodetic data to model the most likely position and extent of the basal Himalayan décollement during the 2015 Gorkha earthquakes.

Published interpretations of the location of the basal décollement exhibit up to ~6 km of variability in the interpreted depth under most of the southern 100 km of the thrust belt, with variability increasing northward (Figure 8). Because different data sources are more reliable for different segments of the profile, we chose an "average" basal décollement as follows: (1) in the southern 30 km of the profile we favor the location of the décollement according to balanced structural cross-sections, at a depth of ~5–7 km (all depths with respect to sea-level). The balanced cross-sections are based on measured thicknesses of the Siwalik Group and surface dip orientations, and reflection seismic profiles verify the location of the décollement (Duvall et al., 2020) so this segment of the décollement is considered to be well constrained (Figure 3). (2) Approximately 30 km north of the southern edge of the profiles, the depth of the décollement is pinned to ~6.5 km by balanced cross-sections, the model of J. R. Elliott et al. (2016), and the broadband seismic profile of Schulte-Pelkum et al. (2005). (3) Between 30 and 60 km, the depth of the décollement in the balanced cross-section interpretations diverges by ~5 km, but at 60 km six of the interpretations place the décollement within a relatively narrow depth range of 10–12.5 km; five of these six interpretations place it between 10 and 11.5 km depth, so we place the average at ~11.0 km. (4) Between 60 and 90 km, the interpretations of Nábělek et al. (2009), Duputel et al. (2016), J. R. Elliott et al. (2016), and DeCelles et al. (2020) place the décollement within a depth window no wider than ~2.5 km, whereas Schulte-Pelkum et al. (2005) and Khanal and Robinson (2013) show the décollement ~5 km deeper over the same region. The average décollement can be divided into four segments, with β varying from ~3° beneath the most proximal part of the foreland basin south of the Main Frontal thrust, to ~3.5° beneath the Chitwan wedge-top basin (Figure 3), to ~6.6° (beneath the Lesser Himalayan Zone), to ~9.1° (north of the Main Central thrust; Figure 8). The analysis below is limited to the southernmost ~80 km of the orogenic wedge. North of ~80 km the surface and décollement slopes increase dramatically, the décollement is located at a depth >18 km below the surface, and brittle behavior of the orogenic wedge and its basal décollement is unlikely (Avouac, 2007; J. R. Elliott et al., 2016; Williams et al., 1994).

To summarize, α varies along strike by about a degree, being lowest (~0.3°) in the region of the Chitwan wedge-top basin and the erosional bight (~1.2°). Northward, α steepens to >7° throughout the south-facing slope of the high Himalaya. The location and shape of the basal décollement is less certain, but its regional mean position suggests β values of ~3.5° beneath Chitwan basin, ~6°–7° beneath the Lesser Himalayan part of the wedge from Chitwan to approximately the trace of the Main Central thrust, steepening to >10° toward the rear of the wedge. Because the location of the basal décollement is so uncertain it is not possible to assess along-strike changes in β that might correspond to those seen in the values of α. It appears that overall taper in the Lesser Himalayan wedge in central Nepal ranges between ~6.5° and 8.5°.

2.4.2. Present Orogenic Wedge Strength

Following Suppe (2007) it is possible to infer overall strengths of the basal décollement and the orogenic wedge based on the assumption that critical wedge taper represents a balance of driving and resisting forces

(see also von Hagke et al., 2014). The analysis assumes mechanical homogeneity and utilizes Dahlen's (1990) equation 99 (using a small-angle approximation), which for a subaerial orogenic wedge simplifies to

$$\propto + \beta = \frac{\beta + \mu_b \left(1 - \lambda_b\right) + \dfrac{S_b}{\rho g H}}{1 + 2\left(1 - \lambda\right)\left[\dfrac{\sin\phi}{1 - \sin\phi}\right] + \dfrac{C}{\rho g H}}, \tag{1}$$

in which S_b and C are pressure-independent components of fault and wedge strengths, respectively, μ_b is the basal coefficient of friction and ϕ is the internal angle of friction, λ_b and λ are the basal and internal pore-fluid pressure ratios, respectively, ρ is the density of rocks that form the wedge, g is gravitational acceleration, and H is the thickness of the wedge. Grouping terms that represent dimensionless fault strength (F, in the numerator) and wedge strength (W, in the denominator), Equation 1 reduces to

$$\propto + \beta = \frac{\beta + F}{1 + W}, \tag{2}$$

which can be rearranged to yield a simple linear relationship

$$\propto = \frac{F}{1 + W} - \frac{W}{1 + W}\beta \tag{3}$$

that represents a line of negative slope, $\propto = \propto_{(\beta=0)} - s\beta$. The intercept ($\propto_{(\beta=0)}$) and slope, s, of this line can be estimated by linear regression of multiple (α, β) pairs in an orogenic wedge (Carena et al., 2002; Suppe, 2007). Further, for subaerial orogenic wedges,

$$W = s \,/\, \left(1 - s\right) \tag{4}$$

and Equation 2 can be rearranged and solved for F as follows:

$$F = \left(\alpha + \beta\right)W + \alpha, \tag{5}$$

which, in the special case of β at $\alpha = 0$, becomes

$$F = \beta_{(\alpha=0)} W \left(\text{Suppe, 2007}\right). \tag{6}$$

Equation 4 may be used by linear regression to determine slope values in situations where multiple α and β values can be measured from a given thrust belt, and Equations 5 and 6 can be used in combination with determination of W, as explained below.

Individual measurements of taper (α and β within a given local sector) in an orogenic wedge can also be used to constrain values of F and W (Suppe, 2007). In central Nepal, four distinct taper districts are relevant: within the Lesser Himalayan Zone of the erosional bight, in the Lesser Himalayan Zone outside of the bight, in the Chitwan wedge-top region, and in the undeformed foredeep directly south of the Main Frontal thrust and the Churia Range (Figure 9). Together these tapers illustrate overall increasing values of both α and β from the front of the Himalaya to its high elevation hinterland region (Figure 9). Table 1 lists values of α, β, $\alpha + \beta$, and corresponding versions of Equation 5 for F as a function of W, which are plotted in Figure 10. Assessment of W can take advantage of the relationship (Dahlen, 1990)

$$W = \left(\sigma_1 - \sigma_3\right) / \sigma_3 = \left(\sigma_1 - \sigma_3\right) / \rho g H. \tag{7}$$

For a Lesser Himalayan wedge of density 2,650 kg m^{-3} and thickness $H = 12$ km, the regional minimum principal stress is approximated by $\rho g H = \sigma_3 = \sigma_N \approx 312$ MPa, and the Coulomb failure criterion provides an estimate of regional maximum shear strength (σ_c) assuming that Byerlee's (1978) law is applicable ($\mu_b = \tan\phi = 0.85$), yielding $\sigma_c = 0.85\sigma_N \approx 265$ MPa.

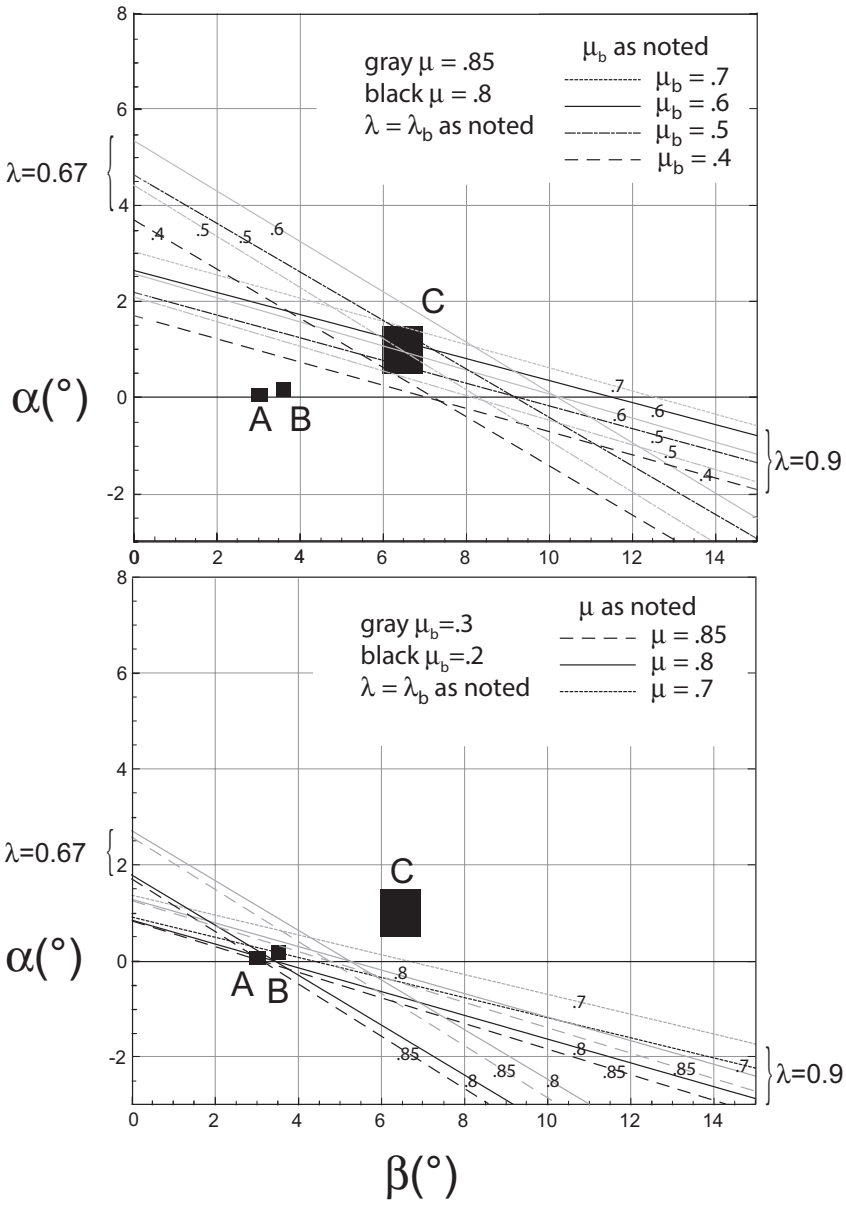

Figure 9. Critical taper diagrams showing surface slope (α) as a function of décollement slope (β) calculated for various combinations of basal strength (μ_b), internal strength (μ), internal pore-fluid pressure ratio (λ), and basal pore-fluid ratio (λ_b). Black rectangles represent α-β combinations in the (A) modern Gangetic foredeep, (B) Chitwan wedge-top basin, and (C) the Lesser Himalayan part of the orogenic wedge north of Chitwan basin.

Table 1
Taper Parameters (in Radians) and Corresponding Equations Used in Figure 10

Location	α	β	$F = (\alpha + \beta)W + \alpha$
Foredeep	0.0017	0.0611	$F = 0.0628W + 0.0017$
Chitwan wedge-top	0.0052	0.0611	$F = 0.0663W + 0.0052$
LH in erosional bight	0.0087	0.1134	$F = 0.1221W + 0.0087$
LH outside erosional bight	0.0279	0.1134	$F = 0.1413W + 0.0279$

The radius, R, of the Mohr circle that corresponds to $\sigma_3 = 312$ MPa and $\sigma_c = 265$ MPa (with $\mu_b = \tan\phi = 0.85$) is $\sigma_c/\cos\phi \approx 347$ MPa. In Mohr space, $\sigma_1 = \sigma_3 + 2R \approx 1{,}006$ MPa. Using these results in Equation 7 produces a maximum W value of 2.2, which applies to all four of the curves in Figure 10 (using $\rho = 2{,}500$ kg m^{-3} and $H = 5$ km for the Chitwan wedge top basin and foredeep wedges). Corresponding maximum values of F for the Lesser Himalayan wedge within and outside of the erosional bight are $F = 0.28$ and $F = 0.34$, respectively (Figure 10; using equations from Table 1). For the Chitwan wedge, Equation 6 produces an F value of 0.13, for $\beta_{(\alpha = 0)} = 3.5°$; the corresponding equation from Table 1 produces $F = 0.15$. These are probably maximum values of F and W for their re-

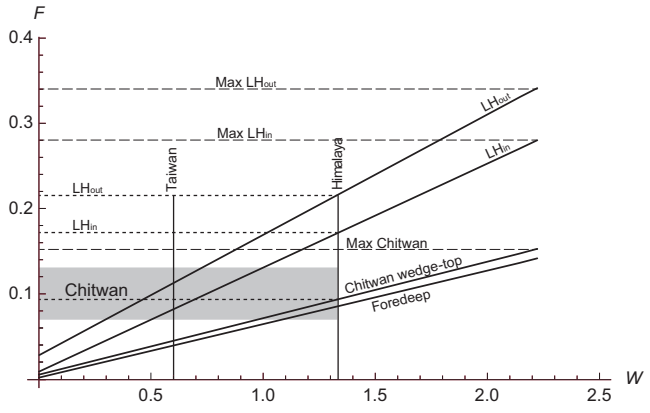

Figure 10. Plot of dimensionless fault strength (F) versus wedge strength (W) (Suppe, 2007). Sloping lines are functions from Table 1. Lines terminate at maximum W values corresponding to $\tan\phi = 0.85$ (Byerlee's law). Horizontal dashed lines indicate corresponding maximum values of F for different sectors of the Himalayan wedge labeled as follows: Max LH_{out}—Lesser Himalayan wedge outside of the erosional bight; Max LH_{in}—Lesser Himalayan wedge inside the erosional bight; Max Chitwan—the sector of the wedge in the Chitwan wedge-top basin area. Gray area represents range of fault strength values determined by Cattin and Avouac (2000), Avouac (2007), and Dal Zilio et al. (2019) for the Himalayan basal décollement. Vertical line labeled Taiwan is wedge strength of the Taiwan orogenic wedge from Suppe (2007). Vertical line labeled Himalaya is value of W calculated for $\phi = 30°$, and dotted horizontal lines indicate corresponding values of F as discussed in text.

spective sectors of the Himalayan orogenic wedge (Figure 10). If we lower the angle of internal friction of the orogenic wedge to 30° ($\mu_b = 0.58$), $W = 1.33$, and $F = 0.09$ for the Chitwan wedge and $F = 0.17$–0.22 for the Lesser Himalayan wedge. W values for the Chitwan and Lesser Himalayan wedges correspond to absolute strength values of 162 and 414 MPa, respectively, which are well within the range of typical upper crustal strengths (Jackson, 2002; Mackwell et al., 1998; Ord & Hobbs, 1989; Tesauro et al., 2015). All of the F values are very low, corresponding to basal shear strengths of ~11–67 MPa. For comparison Suppe (2007) used Equations 4 and 5 and a linear regression of multiple values of α and β for the Taiwan thrust belt to derive a W value of 0.6, and F values of 0.07–0.11. Cattin and Avouac (2000), Avouac (2007), and Dal Zilio et al. (2019) estimated a range of basal friction values in the Himalayan orogenic wedge between 0.07 and 0.13 (Figure 10).

Décollement and wedge strength parameters can also be graphically or analytically inverted from the wedge taper (Figure 9). Many combinations of basal and internal strength and fluid-pressure ratios can create critical taper curves that overlap with the taper values of the four districts of the thrust belt (Figures 9 and 11). The present Lesser Himalayan wedge, both within and outside of the erosional bight, overlaps with typical high basal-friction critical wedges (Figure 11). High-strength wedges (μ = 0.8–0.85), riding on moderately over-pressured to nearly litho-pressured ($\lambda = \lambda_b$ = 0.67–0.9) décollements or décollements with moderate coefficients of basal friction (μ_b = 0.4 to 0.7) can produce tapers that match the Lesser Himalayan wedge taper. In contrast, only wedges with basal décollements characterized by very low coefficients of friction (μ_b = 0.2 to 0.3) and high fluid-pressures ($\lambda = \lambda_b$ = 0.67 to 0.9) can obtain a critical value of taper as low as that in Chitwan basin and in the

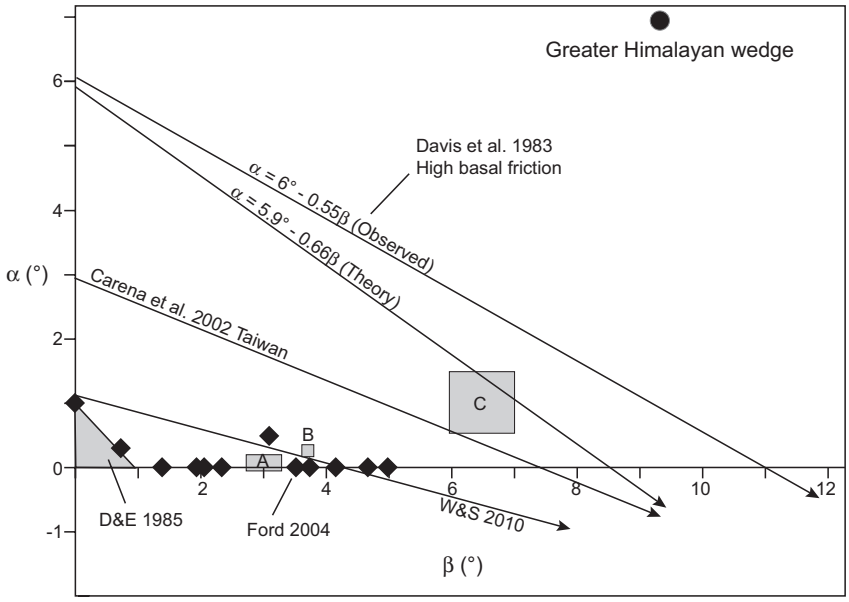

Figure 11. Critical taper solutions for orogenic wedges with very low taper values (D&E: Davis & Engelder, 1985; diamonds: Ford, 2004; W&S: Willett & Schlunegger, 2010) compared with higher basal friction wedges (Taiwan, Carena et al., 2002) and theoretical and experimental high basal friction wedges (Davis et al., 1983). Gray rectangles represent α-β combinations in the (A) modern Gangetic foredeep, (B) Chitwan wedge-top basin, and (C) the Lesser Himalayan part of the orogenic wedge north of Chitwan basin. Black circle is approximate average α-β combination of the Greater Himalayan sector of the orogenic wedge in central Nepal (from Figures 7 and 8).

proximal foredeep (Figure 9). The low-critical-taper frontal parts of the Himalayan wedge in central Nepal have tapers that are comparable to those in salt-based and very low basal-friction wedges (Figure 11; e.g., Dahlen, 1990; D. M. Davis & Engelder, 1985; Ford, 2004; Jaumé & Lillie, 1988; Willett & Schlunegger, 2010). As no evaporites are present in the Siwalik Group, the likely culprit for low-taper criticality in the frontal Himalaya is the localization of the basal décollement in weak shale of the lower member of the Siwalik Group or the underlying Dumri Formation (Chapman & DeCelles, 2015), with or without high fluid pressures. Evidence for high fluid pressures in the Himalayan orogenic wedge includes high electrical conductivity with low V_p/V_s (see Lemmonier et al., 1999; Sheehan et al., 2014); moreover, abundant water in the wedge is expected from metamorphic reactions and foreland sediment compaction beneath and within the wedge (Avouac, 2003, 2007; Lemmonier et al., 1999) as well as the abundant seasonal rainfall (Bettinelli et al., 2008; Chanard et al., 2014).

Taper in the Greater Himalayan sector of the orogenic wedge increases dramatically northward to values that are incompatible with typical brittle critical-taper wedges (Williams et al., 1994), with α values >7° and β values >9° (Figure 11), and thence flattens northward as the topographic surface rolls out onto the Tibetan Plateau. The steep Greater Himalayan south face is relatively narrow (20–40 km, Figure 7) and fits the model results of Williams et al. (1994) for wedges and décollements that are in transition from brittle to ductile behavior. Williams et al. (1994) found that the steep (high α) zone in numerically modeled orogenic wedges is bracketed by points at depth where the lower part of the wedge becomes ductile and where the basal décollement becomes ductile. Over this relatively narrow zone, wedge strength decreases rapidly because the hanging wall rocks have begun to deform ductilely while the décollement remains frictional. As noted by D. Davis et al. (1983), Dahlen (1990), and Avouac (2007) this portion of the Himalayan wedge and its basal décollement are most likely transitioning from brittle-frictional behavior to ductile behavior, with local rapid uplift controlled by rapid erosion and flexural isostatic response above the major footwall ramp on the basal décollement. North of the base of the footwall ramp >20 km below the surface, the basal décollement is weakly coupled and ductilely creeping and the lower, hotter part of the wedge is likely ductile as well, consistent with the locations of the 2015 Gorkha earthquakes and modeling of geodetic data (Figure 5; Ader et al., 2012; Avouac et al., 2015; J. R. Elliott et al., 2016; Stevens & Avouac, 2015).

2.4.3. Paleo-Taper

Although reconstructing paleo-taper, even in a still-active thrust belt such as the Himalaya, is fraught with imponderables, it is nevertheless possible to infer paleo-taper functional states (subcritical, critical, supercritical) based on structural/kinematic and erosional behavior and lithological aspects of the orogenic wedge (e.g., DeCelles & Mitra, 1995). Because orogenic wedges are probably at near-critical state most of the time (Mitra & Boyer, 1986), even minor changes in various parameters may have a strong effect on wedge kinematics (Bettinelli et al., 2008; Mukul, 2010). From a kinematic viewpoint, periods of duplexing and out-of-sequence thrusting are likely signals of an orogenic wedge that has insufficient taper to propagate forward (Avouac, 2007; DeCelles & Mitra, 1995; Fillon, Huismans, van der Beek, & Muñoz, 2013; Gutscher et al., 1996; He et al., 2015; Kukowski et al., 2002; Mitra, 1997; Mitra & Boyer, 2020; Mitra et al., 2010). Conversely, long-distance thrust propagation events may be a response to critical or supercritical taper (DeCelles & Mitra, 1995; Stockmal et al., 2007). Numerical, analytical, and analog models demonstrate that causes of these different behaviors span a wide range of possibilities, including changes in bulk-rock rheology and basal strength, fluid pressures within and at the base of the wedge, changes in erodibility as a function of rock type exposure, changes in climate (especially rainfall), and changes in flexural subsidence (e.g., Buiter, 2012; Carrapa, 2009; Dahlen, 1990; D. Davis et al., 1983; Fillon, Huismans, & van der Beek, 2013; Fillon, Huismans, van der Beek, & Muñoz, 2013; Fuller et al., 2006; Gutscher et al., 1996; Hilley & Strecker, 2004; Jaumé & Lillie, 1988; H. Liu et al., 1992; Roe et al., 2008; Stockmal et al., 2007; Stolar et al., 2007; Storti & McClay, 1995; Tomkin & Roe, 2007; Whipple & Meade, 2004; Willett, 1992; Willett & Schlunegger, 2010; Williams et al., 1994). All of these phenomena are related to both inherent wedge properties and/or external influences such as climate.

The kinematic history of the Himalayan thrust belt in Nepal during Miocene-present time exhibits three general behavioral modes: (1) During the early Miocene, shortening was dominated by long-distance (>100 km) displacements of the Main Central and Ramgarh thrust sheets (DeCelles et al., 2001, 2016, 2020; Long et al., 2011; Robinson & Martin, 2014; Robinson & McQuarrie, 2012; Robinson et al., 2006). (2) Be-

ginning ca. 11 Ma, the Lesser Himalayan duplex began to grow beneath the Ramgarh and Main Central thrust sheets, as duplex horses composed of LHS rocks began to stack up in relatively short-distance thrust displacement events (DeCelles et al., 2016, 2020; Robinson & Martin, 2014; Robinson & McQuarrie, 2012; Robinson et al., 2006). Mid-Miocene duplexing within the interior of the thrust belt was a trans-Himalayan phenomenon (e.g., Bhattacharyya & Mitra, 2009; DeCelles et al., 2001, 2016; Long et al., 2011; Mitra et al., 2010; Robinson & Martin, 2014; Robinson et al., 2006; Webb, 2013), suggesting that an external forcing process was responsible for this change in kinematic behavior. (3) Beginning ca. 5 Ma in Nepal (but possibly earlier in northern India; Meigs et al., 1995; R. Thiede et al., 2017) fault slip was concentrated on thrust faults at the front of the range, including the Main Boundary thrust and, subsequently, thrusts in the Main Frontal thrust system by 2–3 Ma (Mugnier et al., 2004; van der Beek et al., 2006). In the Chitwan sector the Main Frontal thrust propagated ~85 km southward into the foredeep stratigraphy, and subsequent shortening of these rocks amounted to ~42 km (Figure 3).

We interpret the long-distance displacements on the Main Central and Ramgarh thrusts as a sign that the thrust belt was functionally critical to supercritical during early Miocene time, probably because it was composed of relatively strong rocks that were durable in the erosional regime at the surface (e.g., Hilley & Strecker, 2004), and because the rocks within the Main Central and Ramgarh thrust shear zones were relatively weak. Growth of the Lesser Himalayan duplex probably signals a kinematic response to a phase of externally imposed subcritical taper, perhaps in response to increased erosion during intensification of the Indian monsoon ca. 12-11 Ma (Dettman et al., 2001). After ~5 Myr of being held in check by rapid erosion, the thrust front began to propagate forward again via Pliocene-Quaternary slip on the Main Boundary and Main Frontal thrust systems (DeCelles et al., 2020).

2.5. Thermochronology as Proxy for Erosion

Cooling ages from low-T thermochronology can provide information on erosion and hence on tectonic and geomorphic processes (Braun et al., 2006). Thermochronological ages from central Nepal are generally Pliocene and younger, attesting to rapid, high-magnitude erosion (Blythe et al., 2007; Herman et al., 2010; Johnston et al., 2020; Nadin & Martin, 2012; Robert et al., 2011).

Low-temperature thermochronologic ages (apatite fission track [AFT], zircon fission track [ZFT], apatite (U-Th)/He [AHe], and zircon (U-Th)/He [ZHe]) from Nepal are between ~15 and 1 Ma (Blythe et al., 2007; DeCelles et al., 2020; Herman et al., 2010; Nadin & Martin, 2012; Robert et al., 2009, 2011; Sakai et al., 2013; Streule et al., 2012; van der Beek et al., 2016). At regional scale, cooling ages in central Nepal are younger than cooling ages in western Nepal (Figures 6c and 6d). ZHe and AFT ages from central Nepal are mostly <5 Ma with a strong component of AFT ages <2 Ma, whereas ages west of the Kali Gandaki River are >5 Ma and as old as ~14 Ma (Figure 6c). AFT ages of sand samples from the Kali Gandaki River and Modi Khola show that catchments of these rivers are characterized by 8-6 Ma detrital populations (DeCelles et al., 2020); ZFT ages from the Kali Gandaki River are between ~10 and 20 Ma (Bernet et al., 2006). Detrital $^{40}Ar/^{39}Ar$ ages from Central Nepal suggest that erosion was concentrated along a 200 km long by 25 km wide band that overlaps the surface trace of the Main Central thrust (essentially PT_2; Johnston et al., 2020; Wobus et al., 2003).

ZHe ages from Greater Himalayan rocks of the Dadeldhura and Jajarkot klippen in Western Nepal are between ~14 and 10 Ma and AFT ages are between ~9 and 4 Ma (DeCelles et al., 2020). Middle Miocene ages correlate with the timing of emplacement of the Ramgarh thrust (~14-10 Ma) and initial growth of the underlying Lesser Himalayan duplex (DeCelles et al., 2001, 2020; Robinson & McQuarrie, 2012; Robinson et al., 2006). Overall, the low-temperature thermochronologic data suggest rapid erosion of 2–8 km of rock from the region of the erosional bight between ca. 4 Ma and the present, whereas regions west and east of the bight eroded more slowly (Figure 6d).

2.6. Sedimentation in the Foreland

Sedimentation in the foreland basin of southern Nepal and northern India is documented by reflection seismic data and sparse hydrocarbon exploratory wells (Duvall et al., 2018, 2020; Karunakaran & Ranga Rao, 1976; Raiverman et al., 1983; Rao, 1973). Depth to basement is greater than 6 km in the most proximal

parts of the foredeep (Figure 2a). The bulk of the material above basement is Miocene-Pleistocene foreland basin deposits, and the deepest part of the section is likely to be Eocene-lower Miocene deposits with local upper Paleozoic-Cretaceous accumulations (Duvall et al., 2020). Depth to basement decreases southward over a distance of 200 km to ~1,000 m, consistent with deposition in a northward down-flexing foreland basin system (Lyon-Caen & Molnar, 1985). Second-order complexities in the depth contours are interpreted as related to intra- or sub-basinal faults (Duvall et al., 2018; Raiverman et al., 1983). A large southward bulging salient in the basement depth contours exists in the region directly south of the Chitwan salient, with a maximum depth >6,000 m, roughly 2,000 m deeper than in adjacent areas to the east and west (Figure 2a). At least 4,500 m of this depth consists of Miocene-Pleistocene Siwalik Group foredeep facies (Duvall et al., 2018; Friedenreich et al., 1994). Unfortunately, the ages of these deposits are not well resolved, although some authors have reported age picks on seismic profiles (Duvall et al., 2020). Equivalent surface sections of Siwalik Group that have been magnetostratigraphically dated (e.g., Ojha et al., 2009) are incomplete, especially in the poorly consolidated upper part of the section. The thickness distribution of post-lower Siwalik Group strata within Chitwan basin-proper is shown in Figure 2b (Friedenreich et al., 1994). In paleomagnetically dated surface sections nearest to Chitwan basin, located at Bakiya Khola (east) and Tinau Khola (west) (stars on Figure 2a), the boundary between the lower and middle Siwalik members ranges between ca. 11 and 10 Ma (Ojha et al., 2009), so it is likely that the Chitwan basin isopach map reflects deposition of sediments that post-date 11 Ma. Two large concentrations of sediment accumulation >2400 m, separated by a zone of somewhat thinner (by ~200 m) deposits beneath the main channel of the Narayani River, dominate Chitwan basin fill.

3. Synthesis and Working Model

The geology, geomorphology, and climate in central Nepal present an interesting puzzle: How did the front of the thrust belt advance so much farther toward the foreland during Main Frontal thrusting, whereas just prior to that, during Main Boundary thrust activity, the thrust front was evidently strongly inhibited from forward propagation? What are the relationships among the erosional bight, the Lesser Himalayan duplex, excess sedimentation in the foreland basin, and rapid young erosion? It is tempting to associate growth of the Lesser Himalayan duplex with excavation of the erosional bight, insofar as duplexing is commonly considered to be a kinematic signal of a thrust belt in a subcritical state owing to erosion of its internal part (e.g., DeCelles & Mitra, 1995; Fillon, Huismans, van der Beek, & Muñoz, 2013; Konstantinovskaia & Malavieille, 2005; Y. Liu et al., 2020). Two facts, however, refute this interpretation: (1) based on thermochronology the erosional bight most likely post-dates the main phase of growth of the duplex, and (2) the duplex is present along strike over a distance of >1,500 km and is a fundamental structural feature of the Himalayan thrust belt, regardless of the presence or absence of erosional anomalies such as the erosional bight in central Nepal. This is not to imply that the Lesser Himalayan duplex is unrelated to erosion and subcritical taper; on the contrary good arguments can be made that the duplex began to form during a period of intensified monsoonal activity around 12-11 Ma (DeCelles et al., 1998, 2020; Dettman et al., 2001; Robinson et al., 2006). Thermochronological data summarized here, however, indicate that the erosional bight is probably no older than ~4 Ma.

A more general problem is whether duplexing is indicative of subcritical taper. Duplexing experiments generally are not tuned to taper state (e.g., Gutscher et al., 1996; Konstantinovskaia & Malavieille, 2005; Kukowski et al., 2002), and so the idea of duplexing to build taper might be considered as an empirical concept rather than a proven physical requirement. Duplexing is probably best considered a form of internal wedge deformation that takes place in the context of a transition between two different geometrical forms that are both functionally critical, one with lower and one with higher taper (Fillon, Huismans, van der Beek, & Muñoz, 2013; Gutscher et al., 1996).

We propose the following sequence of events in central Nepal to explain the time-space relationships among erosion, foreland sedimentation, and thrust kinematics:

1. (Figure 12a) Between ~14 and 12 Ma the Ramgarh thrust sheet was emplaced on top of a regional low-angle footwall ramp cutting southward upsection from upper Lesser Himalayan rocks to Cenozoic foreland basin deposits (DeCelles et al., 2001, 2020; Robinson & Martin, 2014; Robinson & McQuarrie, 2012; Robinson et al., 2006). Total slip was on the order of 100 km, and the absence of other major

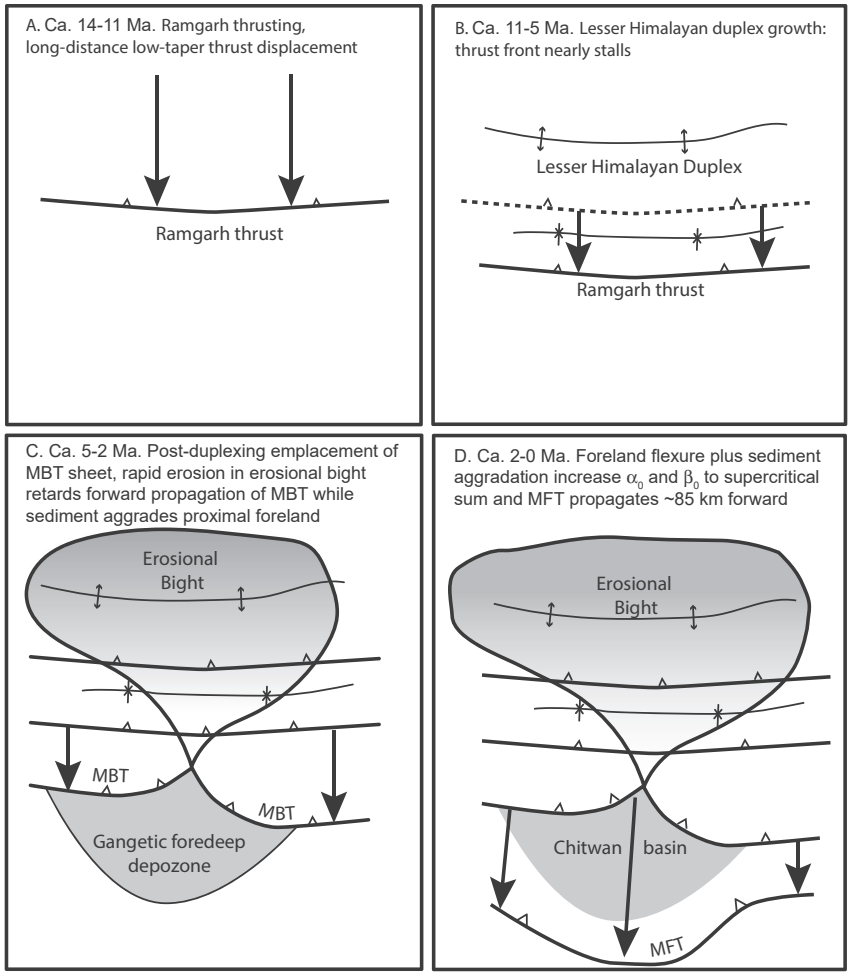

Figure 12. Schematic maps of central Nepal showing the temporal sequence of thrusting, erosion, and sedimentation in the foreland basin system. See text for discussion.

thrusts and shorter wavelength folds suggests that the thrust belt was in a critical to supercritical (stable sliding) state with a relatively low taper angle. This state of behavior (stable sliding with very low regional taper) could have been related to a relatively high internal strength of the wedge (dominated by ortho- and paragneiss) in combination with a weak phyllosilicate-rich basal décollement/shear zone (DeCelles et al., 2020).

2. (Figure 12b) Beginning about 11 Ma, thrust horses of Lesser Himalayan rocks were clipped off of the footwall beneath the Ramgarh thrust by rejoining intra-duplex splay thrusts and the antiformal Lesser Himalayan duplex began to develop. These duplex splays likely fed slip upward and southward into the Ramgarh thrust shear zone, possibly daylighting along the frontal trace of the Ramgarh thrust; no significant break-through thrusts have been documented in the Ramgarh hanging-wall rocks. Duplexing continued until at least 5 Ma, and may be still active (Mendoza et al., 2019). The cause of duplexing was likely rapid erosion owing to a combination of monsoon intensification (Dettman et al., 2001) and regional stripping of relatively durable (Cannon et al., 2018) Greater Himalayan metamorphic rocks and simultaneous regional exposure of structurally underlying much weaker and more easily eroded Lesser Himalayan rocks (DeCelles et al., 2020).
3. (Figure 12c) Beginning around 5 Ma, the Main Boundary thrust became active and juxtaposed Proterozoic Lesser Himalayan strata against upper Miocene-Pliocene strata of the upper Siwalik Group. Conglomerates in the upper Siwalik member contain abundant Lesser Himalayan quartzite clasts, suggesting derivation from the hanging wall of the Main Boundary thrust as well as from older thrust sheets in the duplex (DeCelles et al., 1998; Szulc et al., 2006). No branchline between the Ramgarh and Main

Boundary thrusts has been documented, suggesting that the Main Boundary thrust is not part of the Lesser Himalayan duplex; instead, it probably represents resumption of forward thrust belt propagation after reestablishment of regional critical taper.

4. (Figure 12c) Low-T thermochronological data compiled here (Figures 6c, d) demonstrate that rapid erosion in the central Nepal erosional bight commenced ca. 4–5 Ma, at about the same time as the main phase of Main Boundary thrust slip. Thus, we propose that the Narayani reentrant on the trace of the Main Boundary thrust owes to hinderance of forward propagation of this part of the thrust in response to local, erosionally controlled taper reduction of the Lesser Himalayan part of the orogenic wedge. Although the absence of hanging-wall cutoffs prevents rigorous comparison of Main Boundary thrust slip along strike, simple geometric considerations as discussed above demonstrate that the reentrant reflects less forward propagation of the MBT at that location than along strike to the east and west. Similar behavior of thrust faults in situations with variable along-strike erosion have been modeled and documented in the field (e.g., Graveleau & Dominguez, 2008; Horton, 1999; Leturmy et al., 2000; Y. Liu et al., 2020; Marques & Cobbold, 2002). This type of thrust belt behavior does not require a subcritical stress state: the local decrease in propagation rate on the MBT (and the entire thrust belt) could reflect a net decrease in orogenic wedge material flux owing to the local increase in erosion. This would be manifest as a decrease in wedge growth rate at critical taper.
5. (Figure 12d) Sediment produced by excavation of the erosional bight accumulated in the proximal part of the foreland basin, possibly as a fluvial megafan (Chakraborty et al., 2010; DeCelles & Cavazza, 1999). Addition of this sediment load onto the foreland lithosphere would have augmented the downward flexure of the lithosphere and aggraded the topographic surface, increasing both α_0 and β_0 of the wedge of basin fill in the foredeep outboard of the erosional bight. Slopes on the modern foreland basin surface north and south of the Churia Range (i.e., in the Chitwan wedge-top basin and in the open Gangetic foredeep depozone) are between ~0.1° and 0.3°, providing estimates of α_0 and the value of α that is sufficient for critical behavior, respectively. An estimate of β_0 can be derived from the Miocene to modern isopach data in the Gangetic foredeep (Figure 2a). The isopach pattern indicates that the foredeep fill thickens from 1,000 to ~5,000 m over a south-to-north distance of ~190 km, with some complexity in the 3,000 m isopach contour (possibly due to subsurface faulting). A smoothed curve that captures the endpoints of the thickness profile plots between modeled flexural profiles for a lithosphere with flexural rigidity of 3.0×10^{23} to 1.0×10^{24} Nm flexed beneath half-loads that produce average topography 150–200 km wide and 4 km high (Figure 13). First derivatives of these flexural profiles provide values of β_0, which range between ~2.5° and 4.5° within 50 km of the thrust front (Figure 13). These values of α_0 and β_0 (0.1° and 2.5°–4.5°, respectively) can be compared with an α value of 0.3° and β value of 3.5° in the modern Chitwan area (Figure 3), and average α values of 0.5°–1.6° and average β values of 6°–7° for the Lesser Himalayan part of the thrust belt as previously discussed (Figure 9). Total (initial) taper of the undeformed foredeep is ~2.6°–3.1°, whereas total taper for the Chitwan and Lesser Himalayan parts of the thrust belt is ~4°–8° (Figure 9). It is clear that β_0 is controlled by flexural rigidity of foreland lithosphere and the thickness of sediment in the foredeep (e.g., Boyer, 1995; Ford, 2004; Stockmal et al., 2007).

4. Discussion

4.1. Alternative Mechanisms

Salients and reentrants along the fronts of thrust belts are globally ubiquitous and several mechanisms exist for their development (Macedo & Marshak, 1999; Marshak, 2004; Mitra, 1997; Yonkee & Weil, 2010). Possible alternative mechanisms for the pattern of salients and reentrants along the frontal Nepalese Himalaya include the presence of preexisting structures in Indian basement beneath the foreland basin (e.g., Gahalaut & Kundu, 2012; Godin et al., 2019), along-strike differential strain partitioning, and possible spatial variations in the strength of the frontal part of the basal décollement (see review by Graveleau et al., 2012). Basement buttressing (e.g., Macedo & Marshak, 1999) is unlikely because the reentrants and salients have opposing polarity; if basement features were affecting the Main Frontal thrust, they should have had a similar effect on the Main Boundary thrust. The effect we are discussing operates at ca. 100 km along-strike wavelengths, whereas basement buttressing-induced salients that have been documented in other thrust belts have much larger spacing (e.g., Macedo & Marshak, 1999; Mitra, 1997; Mouthereau et al., 2012; Yonkee & Weil, 2015). Although

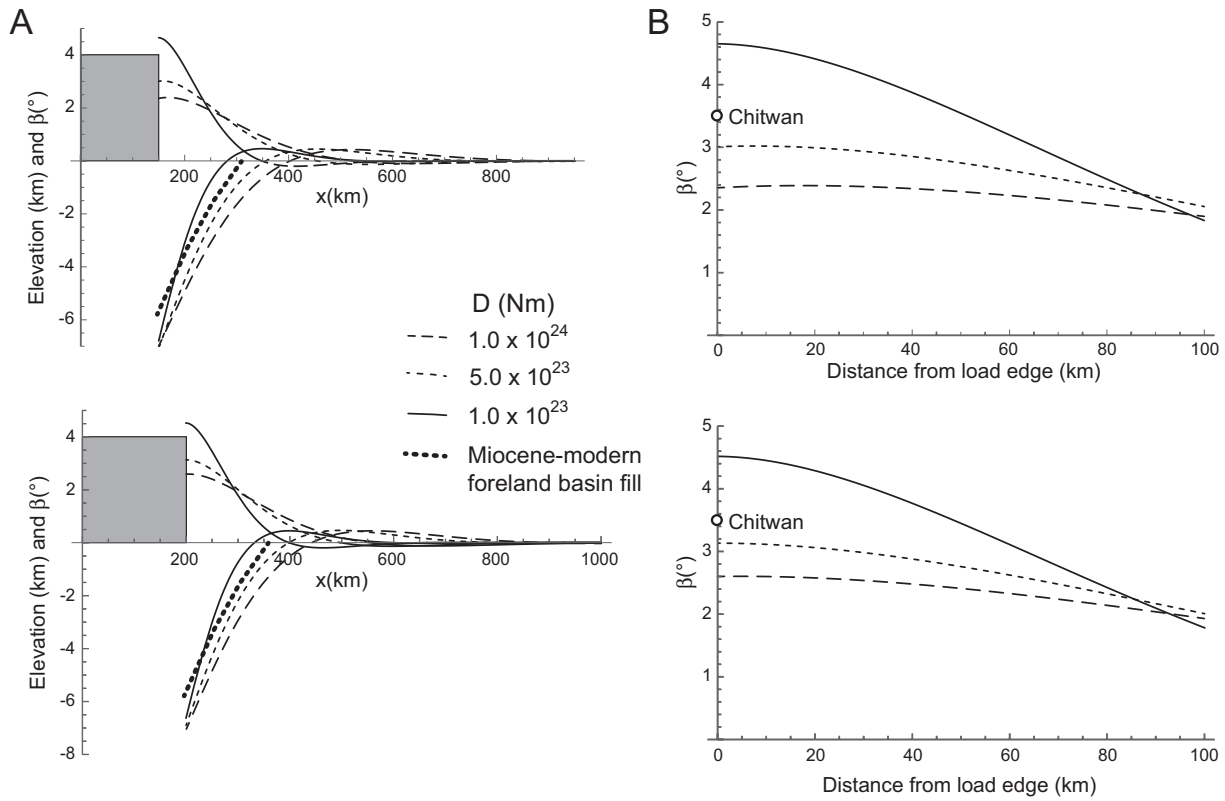

Figure 13. (a) Flexural profiles (lower, upward convex curves) for homogeneous continuous plates of flexural rigidities (D) as listed, flexed under half-loads that would support illustrated topography (depicted as gray boxes); two different loads are shown. Bold dashed curves represent approximate sediment accumulation in the foreland basin deposits of the Siwalik Group (from isopach contours in Figure 2). Upper, concave upward curves represent first derivatives of the flexural profiles, which approximate décollement slope (β). (b) Expanded β plots within 100 km of the thrust belt front, for varying values of D as listed, corresponding to adjacent plots in part (a). White circles represent β value for the Chitwan wedge-top basin (see Figure 3).

structures have been inferred to exist in Indian basement beneath the foreland basin, they are spaced several hundred kilometers apart and do not coincide spatially with the Chitwan salient on the Main Frontal thrust (Gahalaut & Kundu, 2012; Godin & Harris, 2014; Godin et al., 2019; Sastri et al., 1971). Along-strike strain partitioning and large lateral ramps are unlikely causes of the Chitwan phenomenon because major along-strike changes in slip and stratigraphic separation on the Main Frontal and Main Boundary thrusts are not supported by balanced cross-sections and geological maps (e.g., DeCelles et al., 2001, 2020; Khanal & Robinson, 2013; Khanal et al., 2014; Mugnier et al., 1999; Robinson & Martin, 2014; Robinson et al., 2006; Schelling, 1992). Variation of strength in the basal décollement due to lithological or fluid attributes is plausible but would be surprising for its exact coincidence with the Main Boundary thrust reentrant, the erosional bight, and the anomalous thickness of foredeep deposits in the Chitwan area.

4.2. Other Examples and Implications for Himalayan Seismicity

Analog (Leturmy et al., 2000; Mugnier et al., 1997) and analytical/numerical (Fillon, Huismans, van der Beek, & Muñoz, 2013, Fillon, Huismans, & van der Beek, 2013; Stockmal et al., 2007; Willett & Schlunegger, 2010) models illustrate the effect of foredeep sediment accumulation in promoting forward propagation of the front of a thrust belt (Figure 14). In the case of central Nepal, the implication is that erosion of the bight both hindered MBT forward propagation and, eventually, produced the volume of sediment in the foredeep that locally increased flexural subsidence (raising β_0), aggraded the depositional surface (increasing α_0), and elevated the internal strength of the foredeep wedge (Fillon, Huismans, van der Beek, & Muñoz, 2013; Stockmal et al., 2007; Willett & Schlunegger, 2010). When the appropriate values were reached, initial taper on the foredeep wedge became functionally supercritical in the Chitwan region and the Main Frontal thrust, which was becoming active along the whole Himalayan orogenic front, propagated

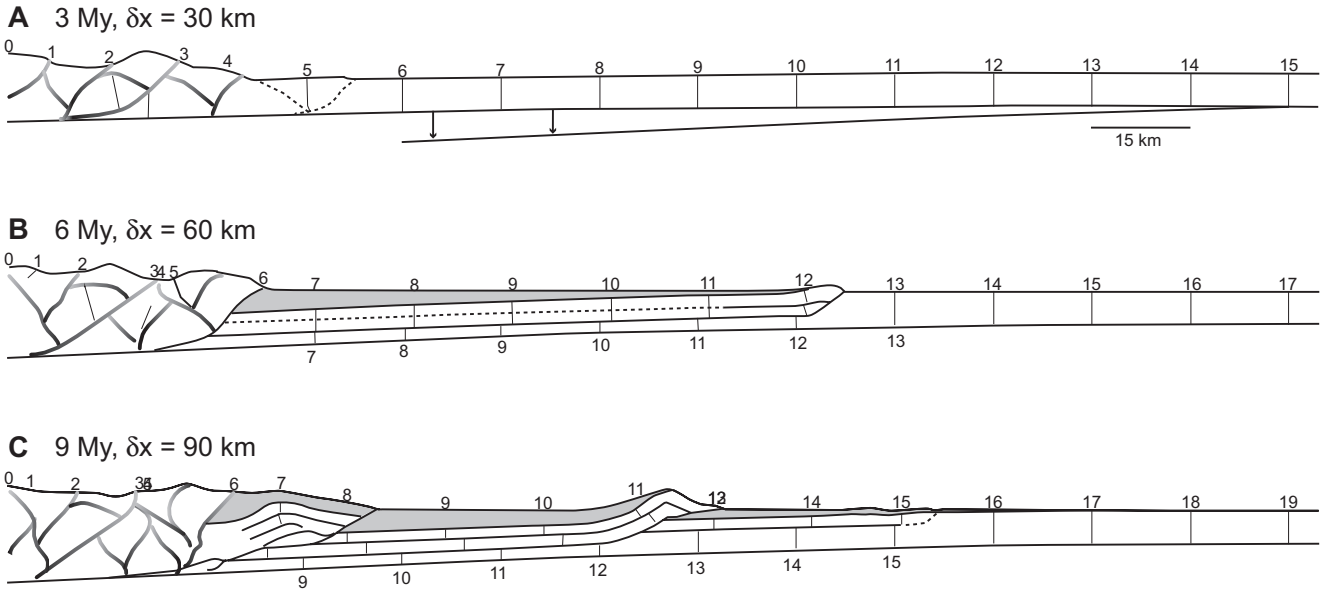

Figure 14. Sequence of Lagrangian-Eulerian frictional-plastic finite element model results abstracted from Stockmal et al. (2007, their Figures 10a–10c). Times indicate time elapsed since initiation of model. Values of δx indicate cumulative distance of shortening. Numbered vertical lines are originally spaced 15 km apart and are progressively disrupted and transposed as the thrust belt advances. No vertical exaggeration. Gray material represents synorogenic sediment, which begins to accumulate in frame (b). Note the close connection between sediment deposition, increased subsidence, and forward propagation of the thrust front. Also note out-of-sequence thrusting that takes place near reference lines 7 and 8 at the 9 My stage (c). Three weak detachment levels are present in this model. Dashed lines indicate incipient slip. Arrows and lowest line in frame (a) represent eventual flexural subsidence that takes place to accommodate sediment load shown in frame (c).

~85 km out to its anomalously far forward location. Similar patterns of localized forward thrust propagation are found in analog models (Graveleau & Dominguez, 2008; Marques & Cobbold, 2002) and have been suggested to control along-strike variations in thrust front propagation in other thrust belts (e.g., DeCelles 1994; Horton, 1999; Leturmy et al., 2000; Y. Liu et al., 2020). Resolution on the timing of the several splay thrusts that disrupted the Chitwan area is too poor to assess whether these faults formed in-sequence or out-of-sequence, but the models of Stockmal et al. (2007) suggest that once the wedge-top basin becomes confined by the new frontal thrust ridge, out-of-sequence thrusts begin to internally shorten the wedge-top (Figures 14b and 14c).

If our model is correct, other regions of the frontal Himalaya where the Main Frontal thrust has propagated anomalously far to the south are candidates for the same combination of erosional, depositional and kinematic events. Reentrants on the Main Boundary thrust and salients on the Main Frontal thrust are common along the length of the Himalayan thrust belt. One obvious region in western Nepal is the area of the Dang and Deukhury wedge-top basins, where the Main Frontal thrust has propagated ~45 km farther south than it has along strike to the east and west, at a scale similar to that of the Chitwan salient (Figures 2 and 5). Although this region is associated with an erosional anomaly that is not as prominent as the one in central Nepal (Figure 5), the Main Boundary thrust does not exhibit a significant reentrant and foreland isopachs do not show anomalously thick sediment accumulation directly south of the salient (Figure 2a). It is possible that the Dang-Deukhury wedge-top area is somewhat older than the still active Chitwan wedge-top area, or that propagation of the Main Boundary thrust was simply not hindered to the same extent as it was at the Narayani River exit canyon. A more likely candidate for a linkage among erosion, deposition, and structural kinematics might be the Karnali River watershed, just west of the Dang-Deukhury wedge-top area (Figure 2). The Karnali area contains excess foredeep sediment, a large river basin (42,890 km^2) with an erosional anomaly, a structural reentrant on the trace of the Main Boundary thrust, and a large wedge-top basin (Figure 2a). Our model would predict that an active blind thrust (shown as a dotted line on Figure 2a) should be present in front of the relatively straight mapped trace of the Main Frontal thrust. A third likely candidate is in eastern Nepal where the Arun River exits the orogenic front and becomes the Kosi River, which is depositing the second largest fluvial megafan in the Himalayan foreland basin (next to that of the

Tista River). Here, the Main Frontal thrust extends 40 km farther into the foreland than along strike, but its trace is buried by the Kosi fan and remains undocumented in the subsurface. Farther southeast, Duvall et al. (2020) reported thrust offset on the blind Bhadrapur thrust ~37 km south of the mapped trace of the Main Frontal thrust. Isopach patterns from this region are complex, however, possibly owing to oblique faults in the subsurface. The thrust belt in all three of these candidate regions is still largely dominated by outcrops of GHS high-grade metamorphic rocks; only the central Nepal erosional bight is virtually stripped of these more resistant (Cannon et al., 2018) rocks. Conceivably, as erosion continues in these other regions, softer rocks of the LHS will become widely exposed and erosional bights will develop accompanied by strong side-effects on orogenic wedge behavior (e.g., Hilley & Strecker, 2004).

Additional candidate areas exist outside of Nepal. In some cases, such as the Salt Range salient in northern Pakistan, coupling of anomalous thrust-belt erosion, Main Boundary thrust reentrant, and the frontal Salt Range thrust (equivalent to the Main Frontal thrust) salient is dramatic. The Salt Range thrust has propagated more than 130 km out from the location of the Main Boundary thrust, and extreme hinterland erosion is associated with the Indus River and its major tributaries. Long-distance forward propagation of the Salt Range thrust is accompanied by structural bivergence and relatively little hanging-wall deformation over a wide region. Overall taper of this part of the orogenic wedge is extremely low (<1.5°) and probably owes to the presence of Eocambrian salt in the basal décollement zone (Baker et al., 1988; Jaumé & Lillie, 1988; Lillie et al., 1987; Pennock et al., 1989).

A second well-documented candidate for the type of complex behavior illustrated by the Chitwan region is the Kangra reentrant in northern India (Powers et al., 1998; T. Singh et al., 2012). In this region, the trace of the Main Boundary thrust exhibits a large reentrant, whereas the Main Frontal thrust propagated ~100 km southwestward into the foreland and its hanging-wall rocks were shortened by ~23 km. Like the Chitwan wedge-top basin, the hanging wall of the Main Frontal thrust is locally disrupted by a belt of small thrust faults and related folds but is otherwise largely undeformed. Powers et al. (1998) showed that β_0 is ~2.5° based on the Janauri-2 and Adampur wells, and total taper in the Kangra reentrant is up to ~4°. The largest erosional anomaly associated with the Kangra reentrant is the Sutlej River drainage basin, which flows into the eastern part of the reentrant after crossing the Main Boundary thrust. The Pakistan and Kangra examples closely resemble the numerical models produced by Stockmal et al. (2007) and Fillon, Huismans, van der Beek, and Muñoz (2013).

Finally, the northeastern part of the Himalayan thrust belt in Arunachal Pradesh provides a smaller but elegant example of Chitwan style erosion-sedimentation-kinematic coupling where the Kameng River exits the thrust belt in a reentrant on the Main Boundary thrust, flows across a small (~15 km wide) wedge-top basin, and exits into the undeformed foredeep (Burgess et al., 2012). The south flank of the wedge-top basin is formed by the Balipara anticline above the Nameri thrust, which is the local name for the Main Frontal thrust (Burgess et al., 2012). The Nameri thrust has a salient form that has propagated ~20 km south of a reentrant on the Tipi thrust, which is an intra-Siwalik Group thrust. Burgess et al. (2012) and Chirouze et al. (2013) provided age constraints of ca. 1 Ma through Holocene time for slip on the Main Frontal thrust system in this area. Upstream in the Kameng River drainage basin, low-temperature cooling ages (mainly AFT ages) demonstrate rapid exhumation during latest Miocene-Pliocene time (DeCelles et al., 2016). Our model would predict that sediment produced by this rapid hinterland erosion accumulated in the foredeep, caused slightly greater flexural subsidence, increased β_0 to a critical value, and the frontal Nameri thrust propagated forward. Very young radiocarbon ages from deformed Quaternary strata on the backlimb of the Balipara anticline suggest the frontal anticline is still active (Burgess et al., 2012; Kumar et al., 2010). We emphasize that none of these other examples has been adequately documented to test the model we present, with perhaps the exception of the Kangra reentrant where ample reflection seismic and well data are available (Powers et al., 1998) and numerous thermochronological studies have been undertaken in the adjacent hinterland region (Deeken et al., 2011; Eugster et al., 2018; Schlup et al., 2011; R. C. Thiede & Ehlers, 2013; R. Thiede et al., 2004, 2017, R. C. Thiede et al., 2005, 2009; Vannay et al., 2004).

Further study of these and other potential examples of linked erosion-deposition-kinematic behavior in the Himalaya is warranted because they could, eventually, shed light on seismic hazard assessments insofar as the largest earthquakes in the Himalaya take place on the basal décollement where and when it feeds slip to the surface along the Main Frontal thrust or blind frontal imbricates (e.g., Avouac, 2003, 2007; Avouac

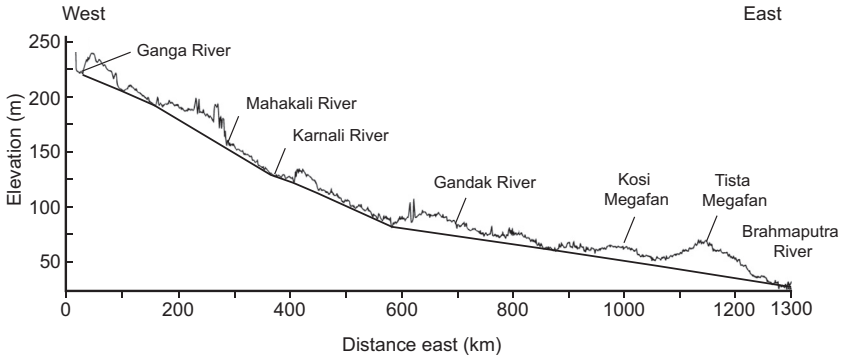

Figure 15. Approximately west-to-east topographic profile ~40–50 km south of the Himalayan topographic front in northern India, from a point 12.4 km north of Muzarfarnagar to a point 8.7 km east of Dhubri on the Brahmaputra River. Major rivers and fluvial megafans are labeled, and lower line connects most of the topographic lows to help emphasize the positive anomalies.

et al., 2015; Bilham, 2019; Bollinger et al., 2014, 2016; Lavé & Avouac, 2001; Lavé et al., 2005; Wesnousky et al., 2017). If hinterland erosion, foreland deposition, and propagation of the Main Frontal thrust are tied together, then additional means of predicting likely regions of future large earthquakes, albeit at coarse temporal resolution, might be provided by detailed studies documenting recent hinterland erosion and linked foreland sedimentation. For example, a longitudinal topographic profile located 40–55 km south of the orogenic front (the approximate average distance of forward propagation of the frontal thrust system) in northern India shows broad topographic swells with amplitudes of 20–50 m and wavelengths of 100–200 km (Figure 15). Two of these are associated with the Kosi and Tista fluvial megafans in the eastern part of the transect, and the others are associated with the Ganga, Mahakali, Karnali, and Gandak Rivers. These areas might be subject to future "break-outs" of the frontal thrust if connected to corresponding regions of rapid erosion. Moreover, recent studies of short-term deformation associated with seasonal rainfall (Bettinelli et al., 2008; Bollinger et al., 2007; Chanard et al., 2014; Gautam & Tiwari, 2007; Panda et al., 2018) and the significant effect of monsoonal (both normal and abnormally intense) precipitation on sediment yield at individual drainage-basin scale (Bookhagen et al., 2005a, 2005b) suggest potential for more refined spatial and temporal predictions.

The work-flow for identifying seismically "primed" regions of the foreland would thus entail (1) documentation of sediment overaccumulations in topographic and subsurface (isopach) data sets; (2) assessment of whether erosional anomalies in the thrust belt are spatially associated with foreland sediment accumulations; (3) compilation or production of low-temperature thermochronological data sets from candidate source drainage basins in the thrust belt—if these data document recent rapid exhumation (ca. <3 Ma) the mechanism we propose could be operating; and (4) assessment of Main Boundary and Main Frontal thrust geometries, with emphasis on reentrant-salient pairs that are in opposite geometric polarity. To these geological data sets could be added detailed paleoseismic and tectonic geomorphologic studies to further assess seismic potential. Areas marked by all of these features should be primed for large earthquakes along the frontal fault system.

5. Conclusions

In central Nepal, Chitwan wedge-top basin is bracketed by the Main Frontal thrust salient and Main Boundary thrust reentrant at the Narayani River. The wedge-top basin formed when the Main Frontal thrust propagated ~85 km outward from the contemporaneous thrust front, and subsequent shortening reduced the width of the basin by about 50%. Foredeep basement in front of the Chitwan salient has been flexed downward >6 km and lies beneath anomalously thick Miocene basin fill, as does the Chitwan wedge-top basin. Low-temperature thermochronological data from the Narayani River drainage basin suggest that rapid Plio-Pleistocene erosion was coeval with slip on the Main Boundary thrust, and this suggests that forward propagation of the Main Boundary thrust was hindered by reduced orogenic wedge taper. At the same time, sediment derived from the Narayani watershed was accumulating in the proximal Gangetic foredeep,

augmenting flexural subsidence in this region. Eventually, both β_0 and α_0 values were increased sufficiently to produce a critical initial taper (*sensu* Boyer, 1995), and the Main Frontal thrust propagated anomalously far into the foredeep. Together with evidence for anomalous precipitation in central Nepal, this suggests that rapid thrust belt erosion, kinematic stalling of the frontal thrust, consequent sedimentation in the undeformed foredeep, and eventual break-out of a new frontal thrust with a salient geometry are linked together in a climate-erosion-sedimentation-kinematic system that accomplishes forward migration of the thrust front in spite of low- to negative-α conditions.

Modern taper of the Himalayan orogenic wedge remains poorly documented, but available data suggest that the wedge in central Nepal can be divided into three segments in the shortening direction: (1) the frontal wedge consists of the proximal foredeep and adjacent wedge-top basins and their structural-topographic boundaries, which together have total taper of ~3°–4° (almost all of which is in β_0 and β); (2) the Lesser Himalayan part of the thrust belt, which has total taper of ~6°–7.5° divided between α values of 1°–1.6° and β values of 5°–6°; and (3) the Greater Himalayan part of the thrust belt, which has widely varying but very high values of α, β, and total taper of >15°. The taper estimates suggest that the frontal part of the orogenic wedge is riding on a very weak, possibly overpressured, basal décollement (though not as weak as the basal décollement in the salt-bearing Pakistan foreland) and the Lesser Himalayan part of the wedge is a typical moderate to high basal-friction critical wedge. The Greater Himalayan part of the orogen is not behaving according to classic Mohr-Coulomb critical taper theory, probably because the lower part of the orogenic wedge and the basal décollement transition to ductile behavior beneath the southern and northern edges, respectively, of the Greater Himalayan Zone.

Insofar as the largest earthquakes in Nepal take place on the Main Frontal thrust system, results reported here suggest that future large earthquakes will be primed by anomalously thick foredeep/wedge-top sediment accumulation, which increases both β_0 and α_0 to values sufficient to allow forward propagation of the thrust front. The same phenomena (augmented flexural subsidence and surface aggradation) are likely to promote seismicity on sectors of the Main Frontal thrust and its extant imbricates.

Data Availability Statement

The published thermochronology data compiled in Figures 6c and 6d are from Blythe et al. (2007), Robert et al. (2009, 2011), Herman et al. (2010), Streule et al. (2012), Nadin and Martin (2012), McCallister et al. (2014), McDermott et al. (2015), van der Beek et al. (2016), Lama Sherpa (2020), and DeCelles et al. (2020), included in Table S1, and in the Reference list.

Acknowledgments
Funding for this research was provided by U.S. National Science Foundation grant EAR1763432. We are grateful to Sean Willett, Glen Stockmal and Saad Haq for stimulating discussions, and to Tank Ojha and Gilby Jepson for help with Figure 6c. Sean Willett and two anonymous reviewers provided critical comments that helped us to improve the manuscript.

References

Adams, B. A., Whipple, K. X., Hodges, K. V., & Heimsath, A. M. (2016). In situ development of high-elevation, low relief landscapes via duplex deformation in the Eastern Himalayan hinterland, Bhutan. *Journal of Geophysical Research: Earth Surface*, *121*, 294–319. https://doi.org/10.1002/2015JF003508

Ader, T., Avouac, J. P., Liu-Zeng, J., Lyon-Caen, H., Bollinger, L., Galetzka, J., et al. (2012). Convergence rate across the Nepal Himalaya and interseismic coupling on the Main Himalayan Thrust: Implications for seismic hazard. *Journal of Geophysical Research*, *117*, B04403. https://doi.org/10.1029/2011JB009071

Alford, D. (1992). *Hydrological aspects of the Himalayan region*. ICIMOD Occasional Paper No. 18, Kathmandu, Nepal, 68 pp.

Almeida, R. V., Hubbard, J., Liberty, L., Foster, A., & Sapkota, S. N. (2018). Seismic imaging of the Main Frontal Thrust in Nepal reveals a shallow décollement and blind thrusting. *Earth and Planetary Science Letters*, *494*, 216–225.

Andermann, C., Bonnet, S., Crave, A., Davy, P., Longuevergne, L., & Gloaguen, R. (2012). Sediment transfer and the hydrological cycle of Himalayan rivers in Nepal (Transfert de sédiments et cycle hydrologique des rivières Himalayennes au Népal). *Comptes Rendus Geoscience*, *344*, 627–635.

Avouac, J.-P. (2003). Mountain building, erosion, and the seismic cycle in the Nepal Himalaya. *Advances in Geophysics*, *46*, 1–80. https://doi.org/10.1016/S0065-2687(03)46001-9

Avouac, J.-P. (2007). Dynamic processes in extensional and compressional settings – Mountain building: From earthquakes to geological deformation. *Treatise on Geophysics*, *6*, 377–439.

Avouac, J.-P., Meng, L., Wei, S., Wang, T., & Ampuero, J.-P. (2015). Lower edge of locked Main Himalayan Thrust unzipped by the 2015 Gorkha earthquake. *Nature Geoscience*, *8*, 708–713.

Baker, D. M., Lillie, R. J., Yeats, R. S., Johnson, G. D., Yousuf, M., & Zamin, A. S. H. (1988). Development of the Himalayan frontal thrust zone: Salt Range, Pakistan. *Geology*, *16*, 3–7.

Bally, A. W., Gordy, P. L., & Stewart, G. A. (1966). Structure, seismic data, and orogenic evolution of southern Canadian Rocky Mountains. *Bulletin of Canadian Petroleum Geology*, *14*, 337–381.

Bernet, M., van der Beek, P., Pik, R., Huyghe, P., Mugnier, J.-L., Labrin, E., & Szulc, A. (2006). Miocene to Recent exhumation of the central Himalaya determined from combined detrital zircon fission-track and U/Pb analysis of Siwalik sediments, western Nepal. *Basin Research*, *18*, 393–412. https://doi.org/10.1111/j.1365-2117.2006.00303.x

Bertrand, M. (1884). Rapports de structure des Alpes de Glaris et du basin houiller du Nord. *Bulletin de la Societe Geologique de France*, *3*, 318–330.

Bettinelli, P., Avouac, J.-P., Flouzat, M., Bollinger, L., Ramillien, G., Rajaure, S., & Sapkota, S. (2008). Seasonal variations of seismicity and geodetic strain in the Himalaya induced by surface hydrology. *Earth and Planetary Science Letters*, *266*, 332–344.

Bhattacharyya, K., & Mitra, G. (2009). A new kinematic evolutionary model for the growth of a duplex – An example from the Rangit duplex, Sikkim Himalaya, India. *Gondwana Research*, *16*, 697–715. https://doi.org/10.1016/j.gr.2009.07.006

Bilham, R. (2019). Himalayan earthquakes: A review of historical seismicity and early 21st century slip potential. In P. J. Treloar & M. P. Searle (Eds.), Himalayan tectonics: A modern synthesis (Vol. 483, pp. 423–482). Geological Society, London, Special Publications.

Bilham, R., Larson, K., & Freymuller, J. (1997). GPS measurements of present-day convergence across the Nepal Himalaya. *Nature*, *386*, 61–64. https://doi.org/10.1038/386061a0

Blythe, A., Burbank, D., Carter, A., Schmidt, K., & Putkonen, J. (2007). Plio-Quaternary exhumation history of the central Nepalese Himalaya: 1. Apatite and zircon fission track and apatite [U-Th]/He analyses. *Tectonics*, *26*, TC3002. https://doi.org/10.1029/2006TC001990

Bohlinger, P., & Sorterberg, A. (2017). A comprehensive view on trends in extreme precipitation in Nepal and their spatial distribution. *International Journal of Climatology*, *38*, 1833–1845. https://doi.org/10.1002/joc.5299

Bollinger, L., Perrier, F., Avouac, J.-P., Sapkota, S., Gautam, U., & Tiwari, D. R. (2007). Seasonal modulation of seismicity in the Himalaya of Nepal. *Geophysical Research Letters*, *34*, L08304. https://doi.org/10.1029/2006GL029192

Bollinger, L., Sapkota, S. N., Tapponnier, P., Klinger, Y., Rizza, M., Van der Woerd, J., et al. (2014). Estimating the return times of great Himalayan earthquakes in eastern Nepal: Evidence from the Patu and Bardibas strands of the Main Frontal thrust. *Journal of Geophysical Research: Solid Earth*, *119*, 7123–7163. https://doi.org/10.1002/2014JB010970

Bollinger, L., Tapponnier, P., Sapkota, S. N., & Klinger, Y. (2016). Slip deficit in central Nepal: Omen for a repeat of the 1344 AD earthquake? *Earth, Planets and Space*, *68*, 1–12. https://doi.org/10.1186/s40623-016-0389-1L

Bookhagen, B., & Burbank, D. W. (2010). Toward a complete Himalayan hydrological budget: Spatiotemporal distribution of snowmelt and rainfall and their impact on river discharge. *Journal of Geophysical Research*, *115*, F03019. http://dx.doi.org/10.1029/2009JF001426

Bookhagen, B., Thiede, R. C., & Strecker, M. R. (2005a). Late Quaternary intensified monsoon phases control landscape evolution in the northwest Himalaya. *Geology*, *33*, 149–152. https://doi.org/10.1130/G20982.1

Bookhagen, B., Thiede, R. C., & Strecker, M. R. (2005b). Abnormal monsoon years and their control on erosion and sediment flux in the high, arid northwest Himalaya. *Earth and Planetary Science Letters*, *231*, 131–146.

Boyer, S. E. (1995). Sedimentary basin taper as a factor controlling the geometry and advance of thrust sheets. *American Journal of Science*, *295*, 1220–1254.

Braathen, A., Bergh, S. G., & Maher, H. D., Jr. (1999). Application of a critical wedge taper model to the Tertiary transpressional fold-thrust belt on Spitsbergen, Svalbard. *Geological Society of America Bulletin*, *111*, 1468–1485.

Braun, J., van der Beek, P., & Batt, G. (2006). *Quantitative thermochronology: Numerical methods for the interpretation of thermochronological data* (1st ed.). New York, NY: Cambridge University Press.

Buiter, S. J. H. (2012). A review of brittle compressional wedge models. *Tectonophysics*, *530–531*, 1–17. https://doi.org/10.1016/j.tecto.2011.12.018

Burbank, D. W., Beck, R. A., & Mulder, T. (1996). The Himalayan foreland basin. In A. Yin & T. M. Harrison (Eds.), *The tectonic evolution of Asia* (pp. 149–188). New York, NY: Cambridge University Press.

Burbank, D. W., Bookhagen, B., Gabet, E. J., & Purkonen, J. (2012). Modern climate and erosion in the Himalaya. *Comptes Rendus Geoscience*, *344*, 610–626.

Burgess, W. P., Yin, A., Dubey, C. S., Shen, Z.-K., & Kelty, T. K. (2012). Holocene shortening across the Main Frontal thrust zone in the eastern Himalaya. *Earth and Planetary Science Letters*, *357–358*, 152–167. https://doi.org/10.1016/j.epsl.2012.09.040

Byerlee, J. D. (1978). Friction of rocks. *Pure and Applied Geophysics*, *116*, 1189–1198.

Caldwell, W. B., Klemperer, S. L., Lawrence, J. F., Rai, S. S., & Ashish (2013). Characterizing the Main Himalayan thrust in the Garhwal Himalaya, India, with receiver function CCP stacking. *Earth and Planetary Science Letters*, *367*, 15–27. https://doi.org/10.1016/j.epsl.2013.02.009

Cannon, J. M., Murphy, M. A., & Taylor, M. (2018). Segmented strain accumulation in the High Himalaya expressed in river channel steepness. *Geosphere*, *14*(3), 1131–1149. https://doi.org/10.1130/GES01508.1

Carena, S., Suppe, J., & Kao, H. (2002). The active detachment of Taiwan illuminated by small earthquakes and its control on first-order topography. *Geology*, *30*, 935–938. https://doi.org/10.1130/0091-7613(2002)030<0935:ADOTIB>2.0.CO;2

Carrapa, B. (2009). Tracing exhumation and orogenic wedge dynamics in the European Alps with detrital thermochronology. *Geology*, *37*, 1127–1130. https://doi.org/10.1130/G30065A.1

Cattin, R. & Avouac, J.-P. (2000). Modeling mountain building and the seismic cycle in the Himalaya of Nepal. *Journal of Geophysical Research*, *105*, 13389–13407.

Chakraborty, T., Kar, R., Ghosh, P., & Basu, S. (2010). Kosi megafan: Historical records, geomorphology and the recent avulsion of the Kosi River. *Quaternary International*, *227*, 143–160.

Chalaron, E., Mugnier, J. L. & Mascle, G. (1995). Control on thrust tectonics in the Himalayan foothills: A view from a numerical model. *Tectonophysics*, *248*, 139–163.

Chanard, K., Avouac, J.-P., Ramillien, G., & Genrich, J. (2014). Modeling deformation induced by seasonal variations of continental water in the Himalaya region: Sensitivity to Earth elastic structure. *Journal of Geophysical Research: Solid Earth*, *119*, 5097–5113. https://doi.org/10.1002/2013JB010451

Chapman, J. B., & DeCelles, P. G. (2015). Foreland basin stratigraphic control on thrust belt evolution. *Geology*, *43*, 579–582.

Chapple, W. M. (1978). Mechanics of thin-skinned fold-and-thrust belts. *Geological Society of America Bulletin*, *89*, 1189–1198. https://doi.org/10.1130/0016-7606(1978)89<1189:MOTFB>2.0.CO;2

Chirouze, F., Huyghe, P., van der Beek, P., Chauvel, C., Chakraborty, T., Dupont-Nivet, G., & Bernet, M. (2013). Tectonics, exhumation, and drainage evolution of the eastern Himalaya since 13 Ma from detrital geochemistry and thermochronology, Kameng River Section, Arunachal Pradesh. *Geological Society of America Bulletin*, *125*, 523–538. https://doi.org/10.1130/B30697.1

Colchen, M. (1999). The Thakkhola-Mustang graben in Nepal and the late Cenozoic extension in the Higher Himalayas. *Journal of Asian Earth Sciences*, *17*, 683–702. https://doi.org/10.1016/S1367-9120(99)00037-1

Dahlen, F. A. (1984). Noncohesive critical Coulomb wedges: An exact solution. *Journal of Geophysical Research*, *89*(B12), 10125–10133. https://doi.org/10.1029/JB089iB12p10125

Dahlen, F. A. (1990). Critical taper model of fold-and-thrust belts and accretionary wedges. *Annual Review of Earth and Planetary Sciences*, *18*, 55–99. https://doi.org/10.1146/annurev.ea.18.050190.000415

Dal Zilio, L., van Dinther, Y., Gerya, T., & Avouac, J.-P. (2019). Bimodal seismicity in the Himalaya controlled by fault friction and geometry. *Nature Communications*, *10*, 48. https://doi.org/10.1038/s41467-018-07874-8

Davis, D., Suppe, J., & Dahlen, F. A. (1983). Mechanics of fold-and-thrusts belts and accretionary wedges. *Journal of Geophysical Research*, *88*(B2), 1153–1172. https://doi.org/10.1029/JB088iB02p01153

Davis, D. M., & Engelder, T. (1985). The role of salt in fold-and-thrust belts. *Tectonophysics*, *119*, 67–89.

DeCelles, P. G. (1994). Late Cretaceous-Paleocene synorogenic sedimentation and kinematic history of the Sevier thrust belt, northeast Utah and southwest Wyoming. *Geological Society of America Bulletin*, *106*, 32–56.

DeCelles, P. G., Carrapa, B., Gehrels, G. E., Chakraborty, T., & Ghosh, P. (2016). Along-strike continuity of structure, stratigraphy, and kinematic history in the Himalayan thrust belt. The view from northeastern India. *Tectonics*, *35*, 2995–3027, https://doi.org/10.1002/2016TC004298

DeCelles, P. G., Carrapa, B., Ojha, T. P., Gehrels, G. E., & Collins, D. (2020). *Structural and thermal evolution of the Himalayan thrust belt in midwestern Nepal*. Geological Society of America Special Paper 547, 77 pp., map insert.

DeCelles, P. G., & Cavazza, W. (1999). A comparison of fluvial megafans in the Cordilleran (Late Cretaceous) and modern Himalayan foreland basin systems. *Geological Society of America Bulletin*, *111*, 1315–1334. https://doi.org/10.1130/0016-7606(1999)111<1315:ACOFMI>2.3.CO;2

DeCelles, P. G., Gehrels, G. E., Najman, Y., Martin, A. J., Carter, A., & Garzanti, E. (2004). Detrital geochronology and geochemistry of Cretaceous – Early Miocene strata of Nepal: Implications for timing and diachroneity of initial Himalayan orogenesis. *Earth and Planetary Science Letters*, *227*, 313–330. https://doi.org/10.1016/j.epsl.2004.08.019

DeCelles, P. G., Gehrels, G. E., Quade, J., Ojha, T. P., Kapp, P. A., & Upreti, B. N. (1998). Neogene foreland basin deposits, erosional unroofing, and the kinematic history of the Himalayan fold-thrust belt, western Nepal. *Geological Society of America Bulletin*, *110*, 2–21. https://doi.org/10.1130/0016-7606(1998)110<0002:NFBDEU>2.3.CO;2

DeCelles, P. G., Kapp, P., Gehrels, G. E., & Ding, L. (2014). Paleocene–Eocene foreland basin evolution in the Himalaya of southern Tibet and Nepal: Implications for the age of initial India-Asia collision. *Tectonics*, *33*(5), 824–849. https://doi.org/10.1002/2014TC003522

DeCelles, P. G., Leary, R. J., & Kapp, P. (2018). Cenozoic basin evolution in the Indus-Yarlung suture zone and High Himalaya. In R. V. Ingersoll, T. F. Lawton, & S. A. Graham (Eds.), Tectonics, sedimentary basins, and provenance: A celebration of William R. Dickinson's career. Geological Society of America Special Paper 540 (pp. 707–739). https://doi.org/10.1130/2018.2540(30)

DeCelles, P. G., & Mitra, G. (1995). History of the Sevier orogenic wedge in terms of critical taper models, northeast Utah and southwest Wyoming. *Geological Society of America Bulletin*, *107*, 454–462. https://doi.org/10.1130/0016-7606(1995)107<0454:HOTSOW>2.3.CO;2

DeCelles, P. G., Robinson, D. M., Quade, J., Ojha, T. P., Garzione, C. N., Copeland, P., & Upreti, B. N. (2001). Stratigraphy, structure, and tectonic evolution of the Himalayan fold-thrust belt in western Nepal. *Tectonics*, *20*, 487–509. https://doi.org/10.1029/2000TC001226

Deeken, A., Thiede, R. C., Sobel, E. R., Hourigan, J. K., & Strecker, M. R. (2011). Exhumational variability within the Himalaya of northwest India. *Earth and Planetary Science Letters*, *305*, 103–114. https://doi.org/10.1016/j.epsl.2011.02.045

Delcaillau, B. (1997). *Les fronts de châines actives. Thèse d'habilitation*. Caen University.

Dettman, D. L., Kohn, M. J., Quade, J., Ryerson, F. J., Ojha, T. P., & Hamidullah, S. (2001). Seasonal stable isotope evidence for a strong Asian monsoon throughout the last 10.7 Ma. *Geology*, *29*, 31–34. https://doi.org/10.1130/0091-7613(2001)029<0031:SSIEFA>2.0.CO;2

Ding, L., Kapp, P., & Wan, X. (2005). Paleocene–Eocene record of ophiolite obduction and initial India-Asia collision, south central Tibet. *Tectonics*, *24*, TC3001. https://doi.org/10.1029/2004TC001729

Duncan, C., Masek, J., & Fielding, E. (2003). How steep are the Himalaya? Characteristics and implications of along-strike topographic variations. *Geology*, *31*(1), 75–78.

Duputel, Z., Vergne, J., Rivera, L., Wittlinger, G., Farra, V., & Hetényi, G. (2016). The 2015 Gorkha earthquake: A large event illuminating the Main Himalayan Thrust fault. *Geophysical Research Letters*, *43*, 2517–2525. https://doi.org/10.1002/2016GL068083

Duvall, M. J., Waldron, J. W. F., Godin, L., & Najman, Y. (2018). *Lateral variability of Cenozoic strata in the Ganga foreland basin of Nepal controlled by Indian basement cross-strike faults*. American Geophysical Union, Fall Meeting, Abstract #T41E-0353.

Duvall, M. J., Waldron, J. W. F., Godin, L., & Najman, Y. (2020). Active strike-slip faults and a new frontal thrust in the Himalayan foreland basin. *Proceedings of the National Academy of Sciences of the United States of America*, *117*(30), 17615–17621. https://doi.org/10.1073/pnas.2001979117

Elliott, D. (1976). The energy balance and deformation mechanisms of thrust sheets. *Philosophical Transactions of the Royal Society*, *A273*, 289–312.

Elliott, J. R., Jolivet, R., González, P. J., Avouac, J.-P., Hollingsworth, J., Searle, M. P., & Stevens, V. L. (2016). Himalayan megathrust geometry and relation to topography revealed by the Gorkha earthquake. *Nature Geoscience*, *9*, 174–180. https://doi.org/10.1038/ngeo2623

Engelder, T. (1990). Smoluchowski's dilemma revisited: A note on the fluid pressure history of the central Appalachian fold-thrust belt. In *The role of fluids in crustal processes, Studies in Geophysics* (pp. 140–147). Washington, DC: National Academy Press.

Eugster, P., Thiede, R. C., Scherler, D., Stübner, K., Sobel, E. R., & Strecker, M. R. (2018). Segmentation of the Main Himalayan Thrust revealed by low-temperature thermochronometry in the western Indian Himalaya. *Tectonics*, *37*, 2710–2726. https://doi.org/10.1029/2017TC004752

Fillon, C., Huismans, R. S., & van der Beek, P. (2013). Syntectonic sedimentation effects on the growth of fold-and-thrust belts. *Geology*, *41*, 83–86.

Fillon, C., Huismans, R. S., van der Beek, P., & Muñoz, J. A. (2013). Syntectonic sedimentation controls on the evolution of the southern Pyrenean fold-and-thrust belt: Inferences from coupled tectonic-surface processes models. *Journal of Geophysical Research: Solid Earth*, *118*, 5665–5680. https://doi.org/10.1002/jgrb.50368

Ford, M. (2004). Depositional wedge tops: Interaction between low basal friction external orogenic wedges and flexural foreland basins. *Basin Research*, *16*, 361–375. https://doi.org/10.1111/j.1365-2117.2004.00236.x

Friedenreich, O., Slind, O. L., Pradhan, U. M. S., & Shrestha, R. B. (1994). Petroleum geology of Nepal. *Canadian Journal of Exploration Geophysics*, *30*, 103–114.

Fuller, C. W., Willett, S. D., & Brandon, M. T. (2006). Formation of forearc basins and their influence on subduction zone earthquakes. *Geology*, *34*, 65–68.

Gahalaut, V. K., & Kundu, B. (2012). Possible influence of subducting reidges on the Himalayan arc and on the ruptures of great and major Himalayan earthquakes. *Gondwana Research*, *21*, 1080–1088.

Gao, R., Lu, Z., Klemperer, S. L., Wang, H., Dong, S., Li, W., & Li, H. (2016). Crustal-scale duplexing beneath the Yarlung Zangbo suture in the western Himalaya. *Nature Geoscience*, *9*, 555–560. https://doi.org/10.1038/ngeo2730

Gautam, U., & Tiwari, D. R. (2007). Seasonal modulation of seismicity in the Himalaya of Nepal. *Geophysical Research Letters*, *34*, L08304. https://doi.org/10.1029/2006GL029192

Godin, L., & Harris, L. B. (2014). Tracking basement cross-strike discontinuities in the Indian crust beneath the Himalayan orogen using gravity data – Relationship to upper crustal faults. *Geophysical Journal International*, *198*, 198–215. https://doi.org/10.1093/gji/ggu131

Godin, L., La Roche, R. S., Waffle, L., & Harris, L. B. (2019). Influence of inherited Indian basement faults on the evolution of the Himalayan orogen. In R. Sharma, I. M. Villa, & S. Kumar (Eds.), Crustal architecture and evolution of the Himalaya-Karakoram-Tibet Orogen (Vol. 481, pp. 251–276). Geological Society, London, Special Publication. https://doi.org/10.1144/SP481.4

Graveleau, F., & Dominguez, S. (2008). Analogue modeling of the interaction between tectonics, erosion and sedimentation in foreland thrust belts. *Comptes Rendus Geoscience*, *340*(5), 324–333. https://doi.org/10.1016/j.crte.2008.01.005

Graveleau, F., Malavieille, J., & Dominguez, S. (2012). Experimental modeling of orogenic wedges: A review. *Tectonophysics*, *538*, 1–66. https://doi.org/10.1016/j.tecto.2012.01.027

Grujic, D., Coutand, I., Bookhagen, B., Bonnet, S., Blythe, A., & Duncan, C. (2006). Climatic forcing of erosion, landscape, and tectonics in the Bhutan Himalayas. *Geology*, *34*, 801–804. https://doi.org/10.1130/g22648.1

Gutscher, M.-A., Kukowski, N., Malavieille, J., & Lallemand, S. E. (1996). Cyclical behavior of thrust wedges: Insights from high basal friction sandbox experiments. *Geology*, *24*, 135–138.

Hauck, M. L., Nelson, K. D., Brown, L. D., Wenjin, Z., & Ross, A. R. (1998). Crustal structure of the Himalayan orogen at ~90° east longitude from Project INDEPTH deep reflection profiles. *Tectonics*, *17*, 481–500. https://doi.org/10.1029/98TC01314

He, D., Webb, A. A. G., Larson, K. P., Martin, A. J., & Schmitt, A. K. (2015). Extrusion vs. duplexing models of Himalayan mountain building 3: Duplexing dominates from the Oligocene to present. *International Geology Review*, *57*, 1–27. https://doi.org/10.1080/00206814.2014.986669

Herman, F., Copeland, P., Avouac, J.-P., Bollinger, L., Mahéo, G., Le Fort, P., et al. (2010). Exhumation, crustal deformation, and thermal structure of the Nepal Himalaya derived from the inversion of thermochronological and thermobarometric data and modeling of the topography. *Journal of Geophysical Research*, *115*, B06407. https://doi.org/10.1029/2008JB006126

Hilley, G. E., & Strecker, M. R. (2004). Steady state erosion of critical Coulomb wedges with applications to Taiwan and the Himalaya. *Journal of Geophysical Research*, *109*, B01411. https://doi.org/10.1029/2002JB002284

Hirschmiller, J., Grujic, D., Bookhagen, B., Coutand, I., Huyghe, P., Mugnier, J.-L., & Ojha, T. (2014). What controls the growth of the Himalayan foreland fold-and-thrust belt? *Geology*, *42*, 247–250. https://doi.org/10.1130/G35057.1

Hodges, K. V. (2000). Tectonics of the Himalaya and southern Tibet from two perspectives. *Geological Society of America Bulletin*, *112*, 324–350. https://doi.org/10.1130/0016-7606(2000)112<324:TOTHAS>2.0.CO;2

Hodges, K. V., Hurtado, J. M., & Whipple, K. X. (2001). Southward extrusion of Tibetan crust and its effect on Himalayan tectonics. *Tectonics*, *20*, 799–809. https://doi.org/10.1029/2001TC001281

Horton, B. K. (1999). Erosional control on the geometry and kinematics of thrust belt development in the Central Andes. *Tectonics*, *18*, 1292–1304.

Hu, S., Garzanti, E., Moore, T., & Raffi, I. (2015). Direct stratigraphic dating of India-Asia collision onset at the Selandian (middle Paleocene, 59 ± 1 Ma). *Geology*, *43*, 859–862. https://doi.org/10.1130/G36872.1

Hubbert, M. K., & Rubey, W. W. (1959). Mechanics of fluid-filled porous solids and its application to overthrust faulting I. *Geological Society of America Bulletin*, *70*, 115–166. https://doi.org/10.1130/0016–7606(1959)70[115:ROFPIM]2.0.CO;2

Hurtado, J. M., Hodges, K. V., & Whipple, K. X. (2001). Neotectonics of the Thakkhola graben and implications for recent activity on the South Tibetan fault system in the central Nepal Himalaya. *Geological Society of America Bulletin*, *113*, 222–240. https://doi.org/10.1130/0016-7606(2001)113<0222:NOTTGA>2.0.CO;2

Ichiyanagi, K., Yamanaka, M. D., Muraji, Y., & Vaidya, B. K. (2007). Precipitation in Nepal between 1987 and 1996. *International Journal of Climatology*, *27*(13), 1753–1762. https://doi.org/10.1002/joc.1492

Islam, M. N., Someshwar Das, S., & Uyeda, H. (2010). Calibration of TRMM derived rainfall over Nepal during 1998-2007. *The Open Atmospheric Science Journal*, *4*, 12–23.

Jackson, J. (2002). Strength of the continental lithosphere: Time to abandon the jelly sandwich? *GSA Today*, *12*(9), 4–10.

Jaumé, S. C., & Lillie, R. J. (1988). Mechanics of the Salt Range-Potwar Plateau, Pakistan: A fold-and-thrust belt underlain by evaporites. *Tectonics*, *7*, 57–71.

Johnston, S. N., Cannon, J. M., & Copeland, P. (2020). Post-Miocene erosion in Central Nepal controlled by midcrustal ramp position, duplex growth, and dynamically maintained elastic strain. *Tectonics*, *39*, e2020TC006291. https://doi.org/10.1029/2020TC006291

Jouanne, F., Mugnier, J. L., Gamond, J. F., Le Fort, P., Pandey, M. R., Bollinger, L., et al. (2004). Current shortening across the Himalayas of Nepal. *Geophysical Journal International*, *157*, 1–14. https://doi.org/10.1111/j.1365-246X.2004.02180.x

Karunakaran, C., & Ranga Rao, A. (1976). *Status of exploration for hydrocarbons in the Himalayan region—Contributions to stratigraphy and structure*. Himalayan Geology Seminar, New Delhi, pp. 1–72.

Khanal, S., & Robinson, D. M. (2013). Upper crustal shortening and forward modeling of the Himalayan fold thrust belt along the Budhi-Gandaki River, central Nepal. *International Journal of Earth Sciences*, *102*, 1871–1891. https://doi.org/10.1007/s00531-013-0889-1

Khanal, S., Robinson, D. M., Mandal, S., & Simkhada, P. (2014). Structural, geochronological and geochemical evidence for two distinct thrust sheets in the 'Main Central thrust zone', the Main Central thrust and Ramgarh–Munsiari thrust: Implications for upper crustal shortening in central Nepal. In S. Mukherjee, R. Carosi, P. A. van der Beek, B. K. Mukherjee, & D. M. Robinson (Eds.), Tectonics of the Himalaya (Vol. 412). Geological Society, London, Special Publications. http://dx.doi.org/10.1144/SP412.2

Konstantinovskaia, E., & Malavieille, J. (2005). Erosion and exhumation in accretionary orogens: Experimental and geological approaches. *Geochemistry, Geophysics, Geosystems*, *6*, Q02006. https://doi.org/10.1029/2004GC000794

Kukowski, N., Lallemand, S. E., Malavieille, J., Gutscher, M.-A., & Reston, T. J. (2002). Mechanical decoupling and basal duplex formation observed in sandbox experiments with application to the Western Mediterranean Ridge accretionary complex. *Marine Geology*, *186*, 29–42.

Kumar, S., Wesnousky, S. G., Jayangondaperumal, R., Nakata, T., Kumahara, Y., & Singh, V. (2010). Paleoseismological evidence of surface faulting along the northeastern Himalayan front, India: Timing, size, and spatial extent of great earthquakes. *Journal of Geophysical Research*, *115*, B12422. http://dx.doi.org/10.1029/2009JB006789

Lama Sherpa, T. Z. (2020). *Tectonic evolution of the Bhumichula plateau: A high elevation low relief surface in western Nepalese Himalaya* (Unpublished M.S. Thesis), University of Arizona, 77 p.

Larson, K., Bürgmann, R., Bilham, R., & Freymueller, J. (1999). The kinematics of the India-Eurasia collision zone from GPS measurements. *Journal of Geophysical Research*, *104*, 1177–1093.

Lavé, J., & Avouac, J.-P. (2001). Fluvial incision and tectonic uplift across the Himalayas of central Nepal. *Journal of Geophysical Research*, *106*, 26561–26591. https://doi.org/10.1029/2001JB000359

Lavé, J., Yule, D., Sapkota, S. N., Basant, K., Madden, C., Attal, M., & Pandey, R. (2005). Evidence for a great medieval earthquake (c. 1100 A.D.) in the central Himalayas, Nepal. *Science*, *141*, 1302–1305.

Lemmonier, C., Marquis, G., Perrier, F., Avouac, J. P., Chitrakar, G., Kafle, B., et al. (1999). Electrical structure of the Himalaya of central Nepal: High conductivity around the mid-crustal ramp along the MHT. *Geophysical Research Letters*, *26*, 3261–3264.

Leturmy, P., Mugnier, J. L., Vinour, P., Baby, P., Colletta, B., & Chabron, E. (2000). Piggyback basin development above a thin-skinned thrust belt with two detachment levels as a function of interactions between tectonic and superficial mass transfer: The case of the Subandean zone (Bolivia). *Tectonophysics*, *320*, 45–67. https://doi.org/10.1016/S0040-1951(00)00023-8

Lillie, R. J., Johnson, G. D., Yousuf, M., Zamin, A. S. H., & Yeats, R. S. (1987). Structural development within the Himalayan foreland fold-and-thrust belt of Pakistan. In C. Beaumont & A. J. Tankard (Eds.), Sedimentary basins and basin-forming mechanisms (Vol. 12, pp. 379–392). Canadian Society of Petroleum Geologists Memoir.

Liu, H., McClay, K. R., & Powell, D. (1992). Physical models of thrust wedges. In K. R. McClay (Ed.), *Thrust tectonics* (pp. 71–81). New York, NY: Chapman & Hall.

Liu, Y., Tan, X., Ye, Y., Zhou, C., Lu, R., Murphy, M. A., et al. (2020). Role of erosion in creating thrust recesses in a critical-taper wedge: An example from Eastern Tibet. *Earth and Planetary Science Letters*, *540*, 116270.

Long, S., McQuarrie, N., Tobgay, T., & Grujic, D. (2011). Geometry and crustal shortening of the Himalayan fold-thrust belt, eastern and central Bhutan. *Geological Society of America Bulletin*, *123*, 1427–1447. https://doi.org/10.1130/B30203.1

Lyon-Caen, H., & Molnar, P. (1985). Gravity anomalies, flexure of the Indian plate, and the structure, support and evolution of the Himalaya and Ganga basin. *Tectonics*, *4*, 513–538.

Macedo, J., & Marshak, S. (1999). Controls on the geometry of fold-thrust belt salients. *Geological Society of America Bulletin*, *111*, 1808–1822. https://doi.org/10.1130/0016-7606(1999)111<1808:COTGOF>2.3.CO;2

Mackwell, S. J., Zimmerman, M. E., & Kohlstedt, D. L. (1998). High-temperature deformation of dry diabase with application to tectonics on Venus. *Journal of Geophysical Research*, *103*, 975–984.

Marques, F. O., & Cobbold, P. R. (2002). Topography as a major factor in the development of arcuate thrust belts: Insights from sandbox experiments. *Tectonophysics*, *348*(4), 247–268. https://doi.org/10.1016/S0040-1951(02)00077-X

Marshak, S. (2004). Salients, recesses, arcs, oroclines, and syntaxes; a review of ideas concerning the formation of map-view curves in fold-thrust belts. In K. R. McClay (Ed.), Thrust tectonics and hydrocarbon systems (Vol. 82, pp. 131–156). American Association of Petroleum Geologists Memoir.

Martin, A. J. (2017). A review of Himalayan stratigraphy, magmatism, and structure. *Gondwana Research*, *49*, 42–80. https://doi.org/10.1016/j.gr.2017.04.031

McCallister, A. T., Taylor, M. H., Murphy, M. A., Styron, R. H., & Stockli, D. F. (2014). Thermochronologic constraints on the late Cenozoic exhumation history of the Gurla Mandhata metamorphic core complex, southwestern Tibet. *Tectonics*, *33*, 27–52. https://doi.org/10.1002/2013TC003302

McDermott, J. A., Hodges, K. V., Whipple, K. X., van Soest, M. C., & Hurtado, J. M., Jr (2015). Evidence for Pleistocene low-angle normal faulting in the Annapurna-Dhaulagiri region, Nepal. *Journal of Geology*, *123*, 133–151.

Meigs, A. J. & Burbank, D. W. (1997). Growth of the South Pyrenean orogenic wedge. *Tectonics*, *16*, 239–258.

Meigs, A. J., Burbank, D. W., & Beck, R. A. (1995). Middle–late Miocene (>10 Ma) formation of the Main Boundary thrust in the western Himalaya. *Geology*, *23*, 423–426. https://doi.org/10.1130/0091-7613(1995)023<0423:MLMMFO>2.3.CO;2

Mendoza, M. M., Ghosh, A., Karplus, M. S., Klemperer, S. L., Sapkota, S. N., Adhikari, L. B., & Velasco, A. (2019). Duplex in the Main Himalayan Thrust illuminated by aftershocks of the 2015 M_w 7.8 Gorkha earthquake. *Nature Geoscience*, *12*, 1018–1022. https://doi.org/10.1038/s41561-019-0474-8

Mitra, G. (1997). Evolution of salients in a fold-and-thrust belt: The effects of sedimentary basin geometry, strain distribution and critical taper. In S. Sengupta (Ed.), Evolution of geological structures in micro- to macro-scales (pp. 59–90). London: Chapman & Hall. https://doi.org/10.1007/978-94-011-5870-1_5

Mitra, G., Bhattacharyya, K., & Mukul, M. (2010). The Lesser Himalayan duplex in Sikkim: Implications for variations in Himalayan shortening. *Journal of the Geological Society of India*, *75*, 289–301. https://doi.org/10.1007/s12594-010-0016-x

Mitra, G., & Boyer, S. E. (1986). Energy balance and deformation mechanisms of duplexes. *Journal of Structural Geology*, *8*, 291–304. https://doi.org/10.1016/0191-8141(86)90050-7

Mitra, G., & Boyer, S. E. (2020). Duplexes as slip transfer zones: Application to the Himalayan fold-thrust belt. *Journal of Asian Earth Sciences*, *190*, 104214. https://doi.org/10.1016/j.jseaes.2019.104214

Molnar, P. M., & Lyon-Caen, H. (1988). Some simple physical aspects of the support, structure, and evolution of mountain belts. In S. P. Clark Jr, B. C. Burchfiel, & J. Suppe (Eds.), Processes in continental lithosphere deformation. Geological Society of America Special Paper 218 (pp. 179–208).

Mouthereau, F., Lacombe, O., & Vergés, J. (2012). Building the Zagros collisional orogen: Timing, strain distribution and the dynamics of Arabia/Eurasia plate convergence. *Tectonophysics*, *532–535*, 27–60.

Mugnier, J. L., Baby, P., Colletta, B., Vinour, P., Bale, P., & Leturmy, P. (1997). Thrust geometry controlled by erosion and sedimentation: A view from analogue models. *Geology*, *25*, 427–430.

Mugnier, J. L., Huyghe, P., Chalaron, E., & Mascle, G. (1994). Recent movements along the Main Boundary thrust of the Himalayas: Normal faulting in an overcritical thrust wedge? *Tectonophysics*, *238*, 199–215. https://doi.org/10.1016/0040-1951(94)90056-6

Mugnier, J. L., Huyghe, P., Gajurel, A. P., & Becel, D. (2005). Frontal and piggy-back seismic ruptures in the external thrust belt of Western Nepal. *Journal of Asian Earth Sciences*, *25*, 707–717.

Mugnier, J. L., Huyghe, P., Leturmy, P., & Jouanne, F. (2004). Episodicity and rates of thrust sheet motion in Himalaya (western Nepal). In K. R. McClay (Ed.), Thrust tectonics and hydrocarbon systems (Vol. 82, pp. 91–114). American Association of Petroleum Geologists Memoir.

Mugnier, J.-L., Leturmy, P., Mascle, G., Huyghe, P., Chalaron, E., Vidal, G., et al. (1999). The Siwaliks of western Nepal 1: Geometry and kinematics. *Journal of Asian Earth Sciences*, *17*, 629–642. https://doi.org/10.1016/S1367-9120(99)00038-3

Mukul, M. (2010). First-order kinematics of wedge-scale active Himalayan deformation: Insights from Darjiling-Sikkim-Tibet (DaSiT) wedge. *Journal of Asian Earth Sciences*, *39*, 645–657. https://doi.org/10.1016/j.jseaes.2010.04.029

Mulugeta, G. (1988). Modeling the geometry of Coulomb thrust wedges. *Journal of Structural Geology*, *10*, 847–859.

Muñoz, J. A., McClay, K. R., & Poblet, J. (1994). Synchronous extension and contraction in frontal thrust sheets of the Spanish Pyrenees. *Geology*, *22*, 921–924.
Nábělek, J. L., Hetényi, G., Vergne, J., Sapkota, S., Kafle, B., Jiang, M., et al. (2009). Underplating in the Himalaya-Tibet collision zone revealed by the Hi-CLIMB experiment. *Science*, *325*, 1371–1374. https://doi.org/10.1126/science.1167719
Nadin, E. S., & Martin, A. J. (2012). Apatite thermochronometry within a knickzone near the Higher Himalaya front, central Nepal: No resolvable fault motion in the past one million years. *Tectonics*, *31*, TC2010. https://doi.org/10.1029/2011TC003000
Ojha, T. P., Butler, R. F., DeCelles, P. G., & Quade, J. (2009). Magnetic polarity stratigraphy of the Neogene foreland basin deposits of Nepal. *Basin Research*, *21*, 61–90. https://doi.org/10.1111/j.1365-2117.2008.00374.x
Ord, A., & Hobbs, B. E. (1989). The strength of the continental crust, detachment zones and the development of plastic instabilities. *Tectonophysics*, *158*, 269–289.
Panda, D., Kundu, B., Gahalaut, V. K., Bürgmann, R., Jha, B., Asaithambi, R., et al. (2018). Seasonal modulation of deep slow-slip and earthquakes on the Main Himalayan Thrust. *Nature Communications*, *9*, 4140. https://doi.org/10.1038/s41467-018-06371-2
Peach, B. N., Horne, J., Gunn, W., Clough, C. T., Hinxman, L. W., & Cadell, H. M. (1888). Report on the recent work of the Geological Survey in the north-west Highlands of Scotland, based on field notes and maps. *Quarterly Journal of the Geological Society of London*, *44*, 378–441.
Peach, B. N., Horne, J., Gunn, W., Clough, C. T., Hinxman, L. W., & Teall, J. J. H. (1907). *The geological structure of the NW Highlands of Scotland*. Memoirs of the Geological Survey of Great Britain.
Pearson, O. N., & DeCelles, P. G. (2005). Structural geology and regional tectonic significance of the Ramgarh thrust, Himalayan fold-thrust belt of Nepal. *Tectonics*, *24*(4), TC4008. https://doi.org/10.1029/2003TC001617
Pennock, E. S., Lillie, R. J., Zamin, A. S. H., & Yousuf, M. (1989). Structural interpretation of seismic reflection data from eastern Salt Range and Potwar Plateau. *American Association of Petroleum Geologists Bulletin*, *73*, 841–857.
Pieri, M. (1989). Three seismic profiles through the Po Plain. In A. W. Bally (Ed.), *Atlas of seismic stratigraphy, volume 3. American Association of Petroleum Geologists Studies in geology 27* (pp. 90–110). AAPG Datapages.
Platt, J. P. (1986). Dynamics of orogenic wedges and the uplift of high-pressure metamorphic rocks. *Geological Society of America Bulletin*, *97*, 1037–1053.
Powers, P. M., Lillie, R. J., & Yeats, R. S. (1998). Structure and shortening of the Kangra and Dehra Dun reentrants, Sub-Himalaya, India. *Geological Society of America Bulletin*, *110*, 1010–1027. https://doi.org/10.1130/0016-7606(1998)110<1010:SASOTK>2.3.CO;2
Price, R. A. (1973). Large-scale gravitational flow of supracrustal rocks, southern Canadian Rockies. In K. A. De Jong & R. Scholten (Eds.), *Gravity and tectonics* (pp. 491–502). New York, NY: Wiley.
Price, R. A. (1988). The mechanical paradox of large overthrusts. *Geological Society of America Bulletin*, *100*, 1898–1908.
Quade, J., Cater, J. M. L., Ojha, T. P., Adam, J., & Harrison, T. M. (1995). Late Miocene environmental change in Nepal and the northern Indian subcontinent: Stable isotopic evidence from paleosols. *Geological Society of America Bulletin*, *107*, 1381–1397. https://doi.org/10.1130/0016-7606(1995)107<1381:LMECIN>2.3.CO;2
Raiverman, V., Kunte, S. V., & Mukherjea, A. (1983). Basin geometry, Cenozoic sedimentation and hydrocarbon prospects in north western Himalaya and Indo-Gangetic plains. *Petroleum Asia Journal*, *6*, 67–92.
Rao, M. B. R. (1973). The subsurface geology of the Indo-Gangetic plains. *Journal of the Geological Society of India*, *14*, 213–242.
Robert, X., van der Beek, P., Braun, J., Perry, C., Dubille, M., & Mugnier, J.-L. (2009). Assessing Quaternary reactivation of the Main Central thrust zone (central Nepal Himalaya): New thermochronologic data and numerical modeling. *Geology*, *37*, 731–734. https://doi.org/10.1130/G25736A.1
Robert, X., van der Beek, P., Braun, J., Perry, C., & Mugnier, J.-L. (2011). Control of detachment geometry on lateral variations in exhumation rates in the Himalaya: Insights from low-temperature thermochronology and numerical modeling. *Journal of Geophysical Research*, *116*, B05202. https://doi.org/10.1029/2010JB007893
Robinson, D. M., DeCelles, P. G., & Copeland, P. (2006). Tectonic evolution of the Himalayan thrust belt in western Nepal: Implications for channel flow models. *Geological Society of America Bulletin*, *118*, 865–885. https://doi.org/10.1130/B25911.1
Robinson, D. M., & Martin, A. J. (2014). Reconstructing the Greater Indian margin: A balanced cross section in central Nepal focusing on the Lesser Himalayan duplex. *Tectonics*, *33*, 2143–2168. https://doi.org/10.1002/2014TC003564
Robinson, D. M., & McQuarrie, N. (2012). Pulsed deformation and variable slip rates within the central Himalayan thrust belt. *Lithosphere*, *4*, 449–464. https://doi.org/10.1130/L204.1
Roe, G. H., Whipple, K. X., & Fletcher, J. K. (2008). Feedbacks among climate, erosion, and tectonics in a critical wedge orogen. *American Journal of Science*, *308*, 815–842.
Sakai, H., Iwano, H., Danhara, T., Hirata, T., & Takigami, Y. (2013). Emplacement of hot Lesser Himalayan nappes from 15 to 10 Ma in the Jumla-Surkhet region, western Nepal, and their thermal imprint on the underlying early Miocene fluvial Dumri Formation. *The Island Arc*, *22*, 361–381. https://doi.org/10.1111/iar.12030
Sastri, V. V., Bhandari, L. L., Raju, A. T. R., & Datta, A. K. (1971). Tectonic framework and subsurface stratigraphy of the Ganga basin. *Journal of the Geological Society of India*, *12*, 222–233.
Schardt, H. (1898). Les régions exotiques du versant Nord des Alpes suisses (Préalpes du Chablais et du Stockhorn et les klippes). *Bulletin Societé Vaudoise Science Natural*, *34*, 113–219.
Schelling, D. (1992). The tectonostratigraphy and structure of the eastern Nepal Himalaya. *Tectonics*, *11*, 925–943. https://doi.org/10.1029/92TC00213
Schelling, D., & Arita, K. (1991). Thrust tectonics, crustal shortening and the structure of the far eastern Nepal Himalaya. *Tectonics*, *10*, 851–862. https://doi.org/10.1029/91TC01011
Schlup, M., Steck, A., Carter, A., Cosca, M., Epard, J.-L., & Hunziker, J. (2011). Exhumation history of the NW Indian Himalaya revealed by fission track and $^{40}Ar/^{39}Ar$ ages. *Journal of Asian Earth Sciences*, *40*, 344–350. https://doi.org/10.1016/j.jseaes.2010.06.008
Schulte-Pelkum, V., Monsalve, G., Sheehan, A., Pandey, M. R., Sapkota, S., Bilham, R., & Wu, F. (2005). Imaging the Indian subcontinent beneath the Himalaya. *Nature*, *435*, 1222–1225. http://dx.doi.org/10.1038/nature03678
Şengör, A. M. C., & Bernoulli, D. (2011). How to stir a revolution as a reluctant rebel: Rudolf Trümpy in the Alps. *International Journal of Earth Science (Geologisches Rundschau)*, *100*, 899–936. https://doi.org/10.1007/s00531-011-0648-0
Sheehan, A. F., de la Torre, T. L., Monsalve, G., Abers, G. A., & Hacker, B. R. (2014). Physical state of Himalayan crust and uppermost mantle: Constraints from seismic attenuation and velocity tomography. *Journal of Geophysical Research: Solid Earth*, *119*, 567–580. https://doi.org/10.1002/2013JB010601

Shen, T., Wang, G., Leloup, P. H., Beek, P., Bernet, M., Cao, K., et al. (2016). Controls on Cenozoic exhumation of the Tethyan Himalaya from fission-track thermochronology and detrital zircon U-Pb geochronology in the Gyirong basin area, southern Tibet. *Tectonics*, *35*, 1713–1734. https://doi.org/10.1002/2016TC004149

Shrestha, M. (2000). Interannual variation of summer monsoon rainfall over Nepal and its relation to Southern Oscillation Index. *Meteorological and Atmospheric Physics*, *75*(1–2), 21–28. https://doi.org/10.1007/s007030070012

Shrestha, S. B., Shrestha, J. N., & Sharma, S. R. (1987a). *Geological Map of Midwestern Nepal*. Kathmandu, Nepal, Survey Department, Topographical Survey Branch, scale 1:250,000.

Simpson, G. (2010). Formation of accretionary prisms influenced by sediment subduction and supplied by sediments from adjacent continents. *Geology*, *38*, 131–134.

Singh, H., Parkash, B., & Gohain, K. (1993). Facies analysis of the Kosi megafan deposits. *Sedimentary Geology*, *85*, 87–113.

Singh, T., Awasthi, A. K., & Caputo, R. (2012). The sub-Himalayan fold-thrust belt in the 1905 Kangra earthquake zone: A critical taper model perspective for seismic hazard analysis. *Tectonics*, *31*, TC6002. https://doi.org/10.1029/2012TC003120

Sinha, R., & Friend, P. F. (1994). River systems and their sediment flux, Indo-Gangetic plains, northern Bihar, India. *Sedimentology*, *41*, 825–845.

Sinha, R., Friend, P. F., & Switsur, V. R. (1996). Radiocarbon dating and sedimentation in the Holocene alluvial sediments of the northern Bihar plains, India. *Geological Magazine*, *133*, 85–90.

Slind, O. L. (1993). *Nepal source and seal study, hydrocarbon assessment of southern Nepal*. Alconsult International Ltd.

Smoluchowski, M. S. (1909). Some remarks on the mechanics of overthrusts. *Geological Magazine*, *6*, 204–205.

Srivastava, P., & Mitra, G. (1994). Thrust geometries and deep structure of the outer and lesser Himalaya, Kumaon and Garhwal (India): Implication for evolution of the Himalayan fold-and-thrust belt. *Tectonics*, *13*, 89–109. https://doi.org/10.1029/93TC01130

Stevens, V., & Avouac, J. (2015). Interseismic coupling on the main Himalayan thrust. *Geophysical Research Letters*, *42*, 5828–5837. https://doi.org/10.1002/2015GL064845

Stöcklin, J. (1980). Geology of Nepal and its regional frame. *Journal of the Geological Society*, *137*, 1–34. https://doi.org/10.1144/gsjgs.137.1.0001

Stockmal, G. S. (1983). Modeling of large-scale accretionary wedge deformation. *Journal of Geophysical Research*, *88*, 8271–8287.

Stockmal, G. S., Beaumont, C., Nguyen, M., & Lee, B. (2007). Mechanics of thin-skinned fold-and-thrust belts: Insights from numerical models. In J. W. Sears, T. A. Harms, & C. A. Evenchick (Eds.), *Whence the Mountains? Inquiries into the evolution of orogenic systems: A volume in Honor of Raymond A. Price. Geological Society of America Special Paper 433* (pp. 63–98). https://doi.org/10.1130/2007.2433(04)

Stolar, D. R., Roe, G. H., & Willett, S. D. (2007). Controls on the patterns of topography and erosion rate in a critical orogen. *Journal of Geophysical Research*, *112*, F04002. https://doi.org/10.1029/2006JF000713

Storti, F. & McClay, K. (1995). Influence of syntectonic sedimentation on thrust wedges in analogue models. *Geology*, *23*, 999–1002.

Streule, M. J., Carter, A., Searle, M. P., & Cottle, J. M. (2012). Constraints on brittle field exhumation of the Everest-Makalu section of the Greater Himalayan Sequence: Implications for models of crustal flow. *Tectonics*, *31*, TC3010. https://doi.org/10.1029/2011TC003062

Suppe, J. (2007). Absolute fault and crustal strength from wedge tapers. *Geology*, *35*, 1127–1130. https://doi.org/10.1130/G24053A.1

Szulc, A. G., Najman, Y., Sinclair, H. D., Pringle, M., Bickle, M., Chapman, H., et al. (2006). Tectonic evolution of the Himalaya constrained by detrital ^{40}Ar-^{39}Ar, Sm-Nd and petrographic data from the Siwalik foreland basin succession, SW Nepal. *Basin Research*, *18*, 375–391. https://doi.org/10.1111/j.1365-2117.2006.00307.x

Tesauro, M., Kaban, M. K., & Mooney, W. D. (2015). Variations of the lithospheric strength and elastic thickness in North America. *Geochemistry Geophysics Geosystems*, *16*(7), 2197–2220. https://doi.org/10.1002/2015GC005937

Thiede, R., Bookhagen, B., Arrowsmith, J. R., Sobel, E., & Strecker, M. (2004). Climatic control on rapid exhumation along the Southern Himalayan Front. *Earth & Planetary Science Letters*, *222*, 791–806. https://doi.org/10.1016/j.epsl.2004.03.015

Thiede, R. C., Arrowsmith, J. R., Bookhagen, B., McWilliams, M. O., Sobel, E. R., & Strecker, M. R. (2005). From tectonically to erosionally controlled development of the Himalayan orogen. *Geology*, *33*, 689–692. https://doi.org/10.1130/G21483.1

Thiede, R. C., & Ehlers, T. A. (2013). Large spatial and temporal variations in Himalayan denudation. *Earth and Planetary Science Letters*, *371–372*, 278–293.

Thiede, R. C., Ehlers, T. A., Bookhagen, B., & Strecker, M. R. (2009). Erosional variability along the northwest Himalaya. *Journal of Geophysical Research*, *114*, F01015. https://doi.org/10.1029/2008JF001010

Thiede, R., Robert, X., Stübner, K., Dey, S., & Faruhn, J. (2017). Sustained out-of-sequence shortening along a tectonically active segment of the Main Boundary thrust: The Dhauladhar Range in the northwestern Himalaya. *Lithosphere*, *9*, 715–725. https://doi.org/10.1130/L630.1

Tomkin, J. H., & Roe, G. H. (2007). Climate and tectonic controls on glaciated critical-taper orogens. *Earth and Planetary Science Letters*, *262*, 385–397. https://doi.org/10.1016/j.epsl.2007.07.040

van der Beek, P., Litty, C., Baudin, M., Mercier, J., Robert, X., & Hardwick, E. (2016). Contrasting tectonically driven exhumation and incision patterns, western versus central Nepal Himalaya. *Geology*, *44*, 327–330. https://doi.org/10.1130/G37579.1

van der Beek, P., Robert, X., Mugnier, J.-L., Bernet, M., Huyghe, P., & Labrin, E. (2006). Late Miocene-Recent exhumation of the central Himalaya and recycling in the foreland basin assessed by apatite fission-track thermochronology of Siwalik sediments, Nepal. *Basin Research*, *18*, 413–434. https://doi.org/10.1111/j.1365-2117.2006.00305.x

Vannay, J.-C., Grasemann, B., Meinert, R., Carter, F. W. A., Baudraz, V., & Cosca, M. (2004). Miocene to Holocene exhumation of metamorphic crustal wedges in the NW Himalaya: Evidence for tectonic extrusion coupled to fluvial erosion. *Tectonics*, *23*, TC1014. https://doi.org/10.1029/2002TC001429

von Hagke, C., Oncken, O., & Evseev, S. (2014). Critical taper analysis reveals lithological control of variations in detachment strength: An analysis of the Alpine basal detachment (Swiss Alps). *Geochemistry, Geophysics, Geosystems*, *15*, 176–191. https://doi.org/10.1002/2013GC005018

Wang, Q., & Zhang, P.-Z. (2001). Present-day crustal deformation in China constrained by global positioning system measurements. *Science*, *294*, 574–577.

Webb, A. A. G. (2013). Preliminary balanced palinspastic reconstruction of Cenozoic deformation across the Himachal Himalaya (northwestern India). *Geosphere*, *9*, 572–587. https://doi.org/10.1130/GES00787.1

Webb, A. A. G., Yin, A., Harrison, T. M., Célérier, J., Gehrels, G. E., Manning, C. E., & Grove, M. (2011). Cenozoic tectonic history of the Himachal Himalaya (north-western India) and its constraints on the formation mechanism of the Himalayan orogen. *Geosphere*, *7*, 1013–1061. https://doi.org/10.1130/GES00627.1

Wells, N. A., & Dorr, J. A. (1987). Shifting of the Kosi River, northern India. *Geology*, *15*, 204–207.

Wesnousky, S. G., Kumahara, Y., Chamlagain, D., Pierce, I. K., Karki, A., & Gautam, D. (2017). Geological observations on large earthquakes along the Himalayan frontal fault near Kathmandu, Nepal. *Earth and Planetary Science Letters*, *457*, 366–375. https://doi.org/10.1016/j.epsl.2016.10.006

Whipple, K. X., & Meade, B. J. (2004). Controls on the strength of coupling among climate, erosion, and deformation in two-sided, frictional orogenic wedges at steady state. *Journal of Geophysical Research*, *109*, F01011. https://doi.org/10.1029/2003JF000019

Willett, S. D. (1992). Dynamic and kinematic growth and change of a Coulomb wedge. In K. R. McClay (Ed.), *Thrust tectonics* (pp. 19–31). London: Chapman & Hall.

Willett, S. D. (1999). Orogeny and orography: The effects of erosion on the structure of mountain belts. *Journal of Geophysical Research*, *104*, 28957–28981.

Willett, S. D., & Schlunegger, F. (2010). The last phase of deposition in the Swiss Molasse Basin: From foredeep to negative-alpha basin. *Basin Research*, *22*, 623–639. https://doi.org/10.1111/j.1365-2117.2009.00435.x

Williams, C. A., Connors, C., Dahlen, F. A., Price, E. J., & Suppe, J. (1994). Effect of the brittle-ductile transition on the topography of compressive mountain belts on Earth and Venus. *Journal of Geophysical Research*, *99*, 19947–19974. https://doi.org/10.1029/94JB01407

Wobus, C. W., Hodges, K. V., & Whipple, K. X. (2003). Has focused denudation sustained active thrusting at the Himalayan topographic front? *Geology*, *31*, 861–864. https://doi.org/10.1130/G19730.1

Xu, Y.-D., Zhang, K.-X., Wang, G.-C., Jiang, S.-S., Chen, F.-N., Xiang, S.-Y., et al. (2012). Extended stratigraphy, palynology and depositional environments record the initiation of the Himalayan Gyirong Basin (Neogene China). *Journal of Asian Earth Sciences*, *44*, 77–93. https://doi.org/10.1016/j.jseaes.2011.04.007

Yin, A., Dubey, C. S., Kelty, T. K., Webb, A. A. G., Harrison, T. M., Chou, C. Y., & Célérier, J. (2010). Geological correlation of the Himalayan orogen and Indian craton: Part 2. Structural geology, geochronology, and tectonic evolution of the eastern Himalaya. *Geological Society of America Bulletin*, *122*, 360–395. https://doi.org/10.1130/B26461.1

Yonkee, W. A., & Weil, A. B. (2010). Reconstructing the kinematics of curved mountain belts: Internal strain patterns in the Wyoming salient, Sevier thrust belt, U.S.A. *Geological Society of America Bulletin*, *122*, 24–49.

Yonkee, W. A., & Weil, A. B. (2015). Tectonic evolution of the Sevier and Laramide belts within the North American Cordilleran orogenic system. *Earth Science Reviews*, *150*, 531–593. https://doi.org/10.1016/j.earscirev.2015.08.001

Zhu, B., Kidd, W. S. F., Rowley, D. B., Currie, B. S., & Shafique, N. (2005). Age of initiation of the India-Asia collision in the east-central Himalaya. *The Journal of Geology*, *113*, 265–285. https://doi.org/10.1086/428805